

Tree Health from Space:
Modeling Urban Tree Health using Multispectral Satellite Imagery in Portland, OR

A Thesis
Presented to
The Division of Mathematics and Natural Sciences
Reed College

In Partial Fulfillment
of the Requirements for the Degree
Bachelor of Arts

Ingrid Tallulah Loraine Zoll

May 2022

Approved for the Division
(Biology)

Aaron Ramirez

Anna Ritz

Acknowledgements

Aaron and Anna

Mama and Nic

Papa and Katherine To my siblings: Forest, thank you for being the coolest big brother I could ever want. Anna, I am so glad that you have become part of my life - the strawberry earrings you made me have become my good luck charm this year. Sabina, thank you for the facetime calls and the junior high drama updates. Wren, thank you for the funny faces and your constant sweet encouragement. Vivian, thank you for the beanie babies and the drawings you sent me.

Mr. Sirovy and Mr. Ruff

KBott

Elin and Victoria, Cayden and Brendan

Mila

Myself!

List of Abbreviations

| | |
|--------------|---|
| ACMA | Bigleaf Maple (<i>Acer macrophyllum</i> , <i>Sapindaceae</i>) |
| ACPL | Norway Maple (<i>Acer platanoides</i> , <i>Sapindaceae</i>) |
| CHM | Canopy Height Model |
| CNH | Coupled Natural-Human (in reference to the CNH2 Project data) |
| DBH | Diameter at Breast Height |
| GIS | Geographic Information System |
| LiDAR | Light Detection and Ranging |
| NDVI | Normalized Difference Vegetation Index |
| PSME | Douglas Fir (<i>Pseudotsuga menziesii</i> , <i>Pinaceae</i>) |
| QGIS | Quantum Geographic Information System |
| RLIS | Regional Land Information System |
| THPL | Western Redcedar (<i>Thuja plicata</i> , <i>Cupressaceae</i>) |

Table of Contents

| | |
|--|----|
| Abstract | 1 |
| Chapter 1: Introduction | 3 |
| 1.1 Urban Forests and Urbanization | 3 |
| 1.2 The Benefits of Urban Forests | 4 |
| 1.3 Environmental Challenges for Urban Trees | 6 |
| 1.4 Urban Forestry in Portland, Oregon | 7 |
| 1.5 Remote Sensing in Urban Landscapes | 8 |
| 1.6 Previous work | 9 |
| 1.7 The Accessibility of Science | 10 |
| 1.8 This Thesis | 12 |
| Chapter 2: Data Resources and Methods | 13 |
| 2.1 Previously Collected Field Data | 14 |
| 2.2 Portland Tree Inventory | 16 |
| 2.2.1 Canopy width and tree height model | 18 |
| 2.3 Satellite Imagery | 18 |
| 2.4 NDVI calculation | 20 |
| 2.5 Canopy Height Model | 21 |
| 2.6 Tree Crown Delineation and Pixel Selection | 21 |
| 2.6.1 Point method | 22 |
| 2.6.2 Radius method | 23 |
| 2.6.3 LiDAR method | 24 |
| 2.7 Modeling Tree Health | 28 |
| Chapter 3: Results | 31 |
| 3.1 Canopy Width and Tree Height Model | 31 |
| 3.2 Health Rating vs. Tree Type and Tree Species | 33 |

| | | |
|--|---|-----------|
| 3.3 | Health Rating vs. NDVI: Point Method Obtained Data | 35 |
| 3.4 | Health Rating vs. NDVI: Radius Method Obtained Data | 36 |
| 3.5 | Health Rating vs. NDVI: LiDAR Method Obtained Data | 37 |
| 3.6 | Method Comparison | 38 |
| 3.7 | Predictive Model | 41 |
| Chapter 4: Discussion | | 51 |
| 4.1 | Strengths and limitations of different delineation techniques | 51 |
| 4.2 | Evaluation of Tree Health Predictions | 54 |
| 4.3 | Impact of Functional Tree Type and Species on Tree Health Assessments | 55 |
| 4.4 | Limitations of Satellite Imaging | 56 |
| 4.5 | Open Source Data and Accessible Science | 56 |
| 4.6 | Future Directions | 57 |
| 4.7 | Conclusion | 58 |
| Appendix A: Supplementary Data | | 59 |
| CNH Project Neighborhoods and Classification | | 59 |
| Variable types for tree inventories | | 59 |
| Scene products and satellite swaths | | 62 |
| Model Tests | | 64 |
| Height model results and predictions | | 66 |
| Tree Height and Crown Width Predictive Model Equations | | 66 |
| Additional Information on Health Predictive Model | | 67 |
| LiDAR model tests | | 68 |
| Predicted Health Rating and Species Counts | | 69 |
| Appendix B: Code | | 71 |
| In Chapter 2: | | 71 |
| Portland Tree Inventory counts and calculations | | 71 |
| Calculating NDVI from satellite imagery | | 72 |
| LiDAR canopy delineation | | 73 |
| In Chapter 3: | | 74 |
| Model for Tree Height and Canopy Width | | 74 |
| Point Method Modeling | | 75 |
| Radius Method Modeling | | 76 |
| LiDAR Method Modeling | | 76 |
| Radius and LiDAR Replications | | 77 |

| | |
|----------------------|----|
| References | 79 |
|----------------------|----|

List of Tables

| | | |
|-----|--|----|
| 2.1 | Final CNH Tree counts | 15 |
| 2.2 | Species counts in Street Trees Database | 17 |
| 2.3 | Species counts in Park Trees Database | 17 |
| 2.4 | 4-band satellite wavelength ranges | 19 |
| 2.5 | Satellite product specifications | 20 |
| 3.1 | Physiological Tree Measurements | 32 |
| 3.2 | Frequency and probability tables of functional tree type and health rating for CNH trees. There is a statistically significant relationship between the two variables ($X^2(2, N=112) = 10.184$, $p = 0.00615$) . . . | 34 |
| 3.5 | Frequency and probability tables of functional tree type and health rating for CNH trees. There is a statistically significant relationship between the two variables ($X^2(2, N=112) = 10.184$, $p = 0.00615$) . . . | 34 |
| 3.8 | Species counts post LiDAR processing | 48 |
| 4.1 | Count of Species and Ratings in final dataset used for LiDAR down-sampled model training | 55 |
| A.1 | | 60 |
| A.2 | Summary of results from various predictive models | 67 |
| A.3 | Statistical values for LiDAR predictive model tests | 68 |

List of Figures

| | | |
|------|---|----|
| 1.1 | The growing inaccessibility of science | 11 |
| 2.1 | Overview of methods and data process | 14 |
| 2.2 | Sampled CNH Trees | 16 |
| 2.3 | Distribution of Health Ratings in the Portland Tree Inventories | 18 |
| 2.4 | Product areas for 2016, 2019, and 2021 satellite scenes | 20 |
| 2.5 | Berkeley Park and CNH trees | 22 |
| 2.6 | CNH trees sampled in Berkeley Park | 23 |
| 2.7 | CNH trees with crown width buffer | 24 |
| 2.8 | LiDAR data clipped to 30m tree buffer | 25 |
| 2.9 | All inventoried trees within the 30m buffer | 25 |
| 2.10 | LiDAR tree crown delineations with selected CNH crowns | 26 |
| 2.11 | Pixel selection method comparison | 26 |
| 2.12 | Geographic extent and random sampling | 27 |
| 2.13 | LiDAR tree crown delineations with selected CNH crowns | 27 |
| 3.1 | Crown width predictive model | 33 |
| 3.2 | Point Method NDVI and Health Rating, by Species | 36 |
| 3.3 | Radius method mean NDVI and health condition by species | 37 |
| 3.4 | NDVI and health condition for LiDAR method | 38 |
| 3.5 | Z-score of NDVI and health rating comparison across methods | 39 |
| 3.6 | Average NDVI comparison between species and methods. | 40 |
| 3.7 | Pixel counts for NDVI calculation, by method, and for sample NDVI. | 41 |
| 3.8 | Confusion matrixes for Point method predictive models | 43 |
| 3.9 | Confusion matrixes for Radius method predictive models | 44 |
| 3.10 | Confusion matrixes for LiDAR method predictive models | 45 |
| 3.11 | Boxplot of probabilities of health group categorization | 46 |
| 3.12 | Probability of Assignment Analysis with Downsampled Data | 47 |
| 3.13 | Confusion matrixes for downsampled predictive models | 48 |

| | | |
|-----|--|----|
| 4.1 | Pixel selection method comparison with numbered trees | 51 |
| 4.2 | Examples of overlapping park and street tree crowns. | 53 |
| 4.3 | Examples of overlapping park and street tree crowns. | 53 |
| A.1 | CNH sampled neighborhoods with classification | 59 |
| A.2 | Satellite scene product swaths for 2016 PlanetScope data | 62 |
| A.3 | Satellite scene product swaths for 2019 PlanetScope data | 62 |
| A.4 | Satellite scene product swaths for 2021 PlanetScope data | 63 |
| A.5 | Model tests for tree height predictions | 64 |
| A.6 | Model tests for tree canopy width predictions | 65 |
| A.7 | Tree height predictive model | 66 |
| A.8 | Graph of species counts for LiDAR health predictions | 69 |

Dedication

To those who speak for the trees

Abstract

Urban trees provide numerous benefits, ranging from aesthetic and environmental to psychological and economical. Tree health is a critical part of urban ecosystem function, and is closely tied to the benefits or lack thereof that urban trees can provide. With over one million trees in Portland's urban forest, conducting field health assessments to understand the dynamics of tree health in Portland is a nearly impossible goal. Due to the size of urban forests and the time consuming practice of field health assessments, recent research into tree health has turned to satellite imagery as a tool for evaluating tree health. This thesis looks to examine the health ratings of four key tree species in Portland (*Acer macrophyllum*, *Acer platanoides*, *Pseudotsuga menziesii*, and *Thuja plicata*) from field data collected in the summer of 2021, and the relationship between health rating and NDVI (Normalized Difference Vegetation Index), which is an index of "greenness" commonly used in remote sensing of vegetation. This thesis tests three different tree canopy delineation and pixel selection techniques for obtaining NDVI to determine which is the most effective for obtaining tree health information and predicting health rating from NDVI. I used an ordinal logistic regression model to predict health ratings of poor, fair or good. These predictions were based on 1) NDVI, 2) NDVI and tree functional type, or 3) NDVI and tree species. The impact of including either tree functional type or tree species in the predictive health model was examined. The most effective predictive model differentiated the predictions by species, and used the LiDAR data. This final model was most effective for the two maple species (ACMA and ACPL), categorizing trees in all three health categories for ACMA, and two health categories for ACPL. The model was ineffective for predicting the health ratings for conifer species.

Chapter 1

Introduction

This thesis looks at urban tree health in Portland, Oregon with the goal of creating a model that predicts tree health rating from NDVI (Normalized Difference Vegetation Index). Additionally, this thesis examines the impact of differentiating by functional tree type or tree species when modeling tree health, as well as the testing and analysis of three different methods of NDVI pixel selection and tree crown delineation.

1.1 Urban Forests and Urbanization

An urban forest is the total population of trees in an urban area. Urban forests are comprised of parks, street trees, landscaped boulevards, green spaces, and any other location where trees can be found in urban spaces. Urban forests are in close proximity to large or dense human populations, have a relatively high diversity of species and forest patch structures as well as both public and private ownership, and their management is often geared toward sustaining tree health and maximizing the potential benefits that trees provide (Robertson et al. 2016). In 2011, urban forests in the United States contained around 74.4 billion trees, which is about a quarter of the total tree population (USDA Forest Service 2011). The US Census bureau reports that, in 2010, nearly 81% of Americans lived in urban areas, up from 79% 10 years earlier. The United Nations predicts that, by 2050, 68% of the world population will live in urban areas (United Nations et al. 2018). As urbanization continues, it becomes increasingly important for both those working to manage urban forests and residents of urban areas to understand the dynamics and health of urban forests in order to retain and protect the numerous benefits they provide.

1.2 The Benefits of Urban Forests

Urban forests and urban trees have numerous benefits, which range from environmental to economic. The environmental benefits of urban trees include numerous forms of pollution removal from both water and air. In undeveloped areas, most of the precipitated water is absorbed into the earth. However, due to the high amount of impervious surfaces such as sidewalks, streets, and parking lots in urban areas, rain and snowmelt are unable to soak back into the earth and become stormwater runoff instead. This runoff flows over developed impervious surfaces and picks up trash, yard waste, dirt, and many other potentially harmful chemicals and pollutants. It is then deposited in streams, rivers, wetlands, and other bodies of water that are damaged by polluted runoff. Green infrastructure like urban trees help in reducing the volume and rate of runoff by allowing more precipitation to be soaked into the earth. Research has shown that the presence of street trees also has a positive impact in reducing stormwater runoff volume (US EPA 2020). A 2021 study conducted in Fond du Lac, Wisconsin, showed that the removal of street trees increased the volume of stormwater runoff by 4% (Selbig et al. 2021). The study calculated that on a per-tree basis for each square meter of canopy that was removed, 66 liters of rainfall could have been intercepted and stored by the street trees. This results in an annual runoff volume reduction estimated at 6,376 liters per tree. In addition to benefiting the land, urban trees can also provide benefits to the atmosphere.

Urban trees also remove pollutants from the air. Numerous studies have shown that trees can remove many different pollutants (O₃, PM10, NO₂, SO₂, CO) by uptake via leaf stomata. Pollutant particles can also be collected and stored on a tree's surface. Urban trees provide a total annual air pollution removal of 711,000 tons, which is valued at \$3.8 billion (David J. Nowak et al. 2006). Cities with higher levels of tree canopy cover have higher rates of pollution removal by trees, and longer on-leaf growing periods of trees lead to more pollution removal as well. While the removal of air pollution by urban trees results in the improvement of air quality, trees also help mitigate climate change, improve atmospheric conditions and air quality through carbon sequestration.

The increase of atmospheric carbon dioxide from human sources is one of the primary drivers of global climate change. In 2019, U.S. greenhouse gas emissions totaled 6,558 million metric tons of carbon dioxide equivalents. In the same year, the city of Portland's carbon emissions totaled around 55,000 metric tons of carbon dioxide equivalents (City of Portland 2020). Rural and urban forests, as well as other

natural and nature based carbon sinks have been suggested as a method of mitigating greenhouse gas emissions of cities in order to reduce the impacts of global climate change (Lazarus et al. 2013). These natural carbon sinks capture atmospheric carbon dioxide during photosynthesis and store the carbon as biomass, releasing oxygen back into the atmosphere. Multiple scholars estimate that urban trees in the United States currently store over 708 million tons of carbon, and capture another 28.2 million tons of carbon per year, which is approximately 0.05% of annual carbon dioxide emissions in the United States (David J. Nowak et al. 2002, 2013; Safford et al. 2013). The current carbon storage of urban trees is valued at more than \$50 billion, with carbon sequestration valued at an additional \$2 billion per year (David J. Nowak et al. 2013). The environmental benefits of urban trees can result in economic advantages under future carbon trading schemas, but there are other unique economic and social benefits that urban trees provide.

Residents of urban areas experience the benefits of urban trees most immediately through the beauty and visual stimulation they provide. Aesthetics alone are a large driver in the plantings of urban trees. Studies have found that trees are one of the main contributors to positive visual aesthetic quality of residential areas, and that large trees contribute more to perceived beauty than smaller trees (H. Schroeder et al. 1983; Herbert W. Schroeder 2011; Herbert W. Schroeder et al. 1987). The positive impacts of urban trees goes far beyond their visual contributions.

Numerous studies have shown that people living near urban forests live longer, experience better mental health, and self-rate their overall health higher than people who do not live near urban forests (James et al. 2015). Residents of two different towns in Germany visited urban forests and green spaces more frequently after the beginning of the COVID-19 pandemic, which contributed significantly to the residents' well-being (Beckmann-Wübbelt et al. 2021). Research into the psychological benefits of urban trees shows that teenage girls who spend more time around trees and other sources of nature and vegetation have higher levels of self-discipline, and children with diagnosed attention deficit disorder show improved focus and ability to learn after spending time outside (Taylor et al. 2001, 2002).

Additionally, urban trees provide numerous economic benefits on both a nation wide and an individual scale. Urban tree canopy cover positively impacts residential property values. In Athens, Georgia, landscaping with trees results in a 3.5%–4.5% increase in home sale price (Anderson et al. 1988). In Ramsey and Dakota Counties, Minnesota, researchers found that a 10% increase in tree cover within 100m of a house increases the average home price by 0.5% (Sander et al. 2010). Both summer

cooling and winter heating demands can be reduced through shading and wind speed reduction by urban trees which lowers energy costs (David J. Nowak et al. 2010). A 2009 study of 460 single-family homes in Sacramento, California showed that tree cover on the south and west sides of houses reduced summer electricity use by 5.2%, whereas trees on the north side of a house increased electricity use by 1.5% (Donovan et al. 2009). A more recent study conducted in the city of Thessaloniki in northern Greece found that the cooling potential of street trees is directly related to the foliage density and the shade provided can lower temperatures up to 5 degrees C, leading to energy savings of up to 54% (Tsoka et al. 2021). All of these benefits are dependent on the health of the tree and trees in poor health will be unable to provide the same level and quality of benefits that a healthy tree can.

1.3 Environmental Challenges for Urban Trees

Human activities have impacted and altered the Earth's climate and land surface at a fundamental level. Some outcomes of these fundamental changes include elevated temperatures and prolonged droughts (Huang et al. 2019). These extreme droughts can trigger extensive forest die-off as well as increased tree and shrub mortality rates, which has impacted forests and woodlands on all vegetated continents. Remote sensing research on the impacts of droughts has shown that the impacts of a drought can produce a suppression of forest canopy greenness, which relates to a failing of plant ecophysiological processes and a reduction of chlorophyll. Droughts are predicted to occur more frequently and have higher intensities as climate change continues to progress.

The impacts of climate change and the environmental challenges that all trees will face is even more extreme in urban areas. The multiple economic, environmental and quality of life, health benefits that are provided by urban trees are dependent on tree health. Urban trees are generally more stressed than those in rural areas due to the adverse growing conditions they face. This includes higher temperatures, additional soil compaction, root zone restrictions, and extreme variations in environmental conditions such as wind speed and sunlight level (Flint 1985; Ward et al. 2007). Monitoring and tracking tree health over time is an essential component for the ability to model and predict the future changes that will occur. Research into the remote sensing of health indicators of forest die-off has shown that vegetation greenness metrics, such as NDVI, reflect the changes that occur with tree die-off (Breshears et al. 2005; Byer et al. 2017). In order to work towards understanding these changes

and how to mitigate the impacts of forest die-off, it is extremely important to understand the current health dynamics of urban forests at a city-wide level, and carefully track changes in urban forest health over time.

1.4 Urban Forestry in Portland, Oregon

Portland is one of many cities to create tree inventories in the last 25 years, with the goal of better understanding the urban forest. Over a period of 9 years, 2,000 volunteers along with members of Portland's Urban Forestry team inventoried Portland's 245,000 park and street trees (DiSalvo et al. 2017; Portland Urban Forestry 2019). In addition to basic physical and environmental variables such as tree height, diameter, and location, volunteers also visually assessed the health condition of each tree, and categorized it as good, fair, poor, or dead. Portland inventoried the 218,602 street trees between 2010 and 2016, and 25,740 park trees between 2017 and 2019. Portland Urban Forestry estimates that Portland's parks contain upwards of 1.2 million trees, but the tree inventory project only inventoried trees in developed portions of parks. Portland Urban Forestry estimates that Portland's street trees produce an estimated \$28.6 million annually in environmental and aesthetic benefits, with a full replacement value of \$753 million (DiSalvo et al. 2017). Portland's inventoried park trees have an estimated worth of \$128 million (Portland Urban Forestry 2019).

While Portland's tree inventories are spectacular resources which help shed light on the urban tree population in Portland and the benefits it can provide, there are limitations to the information available through the inventories. One drawback of the inventories is that volunteers were only able to inventory trees on public land, which excluded any trees growing in yards or other privately owned areas. Since only developed portions of parks were inventoried, roughly 98% of Portland's park trees, which are in natural and "undeveloped areas", were not inventoried. Additionally, since the inventories were collected over a 9 year period, the collected health assessments for many trees are no longer reliable or representative of present day conditions. They represent data from a range of 9 years and in the 11 years since inventory collection began much has changed.

Measuring urban tree health through field surveys can be extremely time and labor intensive. It requires the collection of detailed data on numerous environmental variables, as well as extensive groundwork to conduct the field surveys. To collect Portland's tree inventories, more than 2,000 volunteers collectively spend upwards of 25,000 hours in the field. Additionally, in order to get a good picture of changes

in tree health over time, trees need to be revisited numerous times over the study period. Remote sensing data from satellite imagery can be used to locate and map trees in both urban and rural areas, as well as monitor tree health.

1.5 Remote Sensing in Urban Landscapes

While the term “remote sensing” was first used in the 1960s, the first aerial images were taken in the 1850s from hot air balloons. Later, small cameras were attached to kites and even pigeons to capture aerial images. With the development of airplanes in the early 20th century, images were able to be taken from higher altitudes, providing aerial views of larger surface areas (Moore 1979). Aerial images taken from planes provided essential military reconnaissance during both World War I and II. The first environmental applications of aerial imagery began in the 1930s, when the Agriculture Department began to use aerial photography to map and catalog farmland in the United States. Soon after, aerial imagery became a tool for conservation and land planning purposes. Capturing aerial images from planes was the primary method of capturing images of the earth’s surface until the early 1960s. Since the first satellite was launched in 1957, the technical capabilities of satellites has greatly increased, along with the types and applications of satellite-collected data (Khorram 2012). Within the field of forestry and ecology, remote sensing has numerous applications, from measuring the cover and structure of vegetation, to examining biodiversity and soil characteristics of specific areas. Additionally, remote sensing measurements can be used to calculate and monitor changes in forest density, which is critical for determining the fuel load and forest health in regards to fire risk.

One of the most commonly used remote sensing metrics used to measure forest health is the Normalized Difference Vegetation Index (NDVI), which is calculated from the red and near infrared (NIR) bands from remote sensing imagery (Section 2.4). Vegetation that is photosynthetically active absorbs most of the red light and reflects much of the near infrared light. Conversely, vegetation that is dead or stressed reflects more red light and absorbs more near infrared light. Biologically, NDVI can be interpreted as the fraction of absorbed photosynthetically active radiation. A value closer to 1 indicates vegetation that is more photo-synthetically active and greener, which can be used as a proxy for vegetation health. NDVI is not a diagnostic tool of vegetation health, but can be used as an indicator of health for further analysis. Studies have shown that NDVI is highly correlated with chlorophyll content. Specifically, NDVI has a near-linear relationship to the chlorophyll content of soybean crops

(Tucker 1979; Myneni et al. 1995).

Especially when the goal is monitoring tree health changes over time, remote sensing data eliminates the need for repeated sampling over long time periods, since satellite images are taken at regular intervals as the satellites continually orbit the earth. With the availability and accuracy of aerial imagery increasing as these technologies continue to advance, remote sensing is becoming an important and effective method for mapping, monitoring, and analyzing tree health on an individual tree scale (Xiao et al. 2005).

1.6 Previous work

Xiao et al. (2005) used multispectral remote sensing data paired with field collected tree health data with the goal of mapping tree health on the University of California Davis campus. Field data on 81 campus trees was collected in the summer of 2004, and the health of the trees was classified as “healthy” or “unhealthy.” Additionally, a second dataset of 1,186 trees was collected which included randomly selected trees to check the accuracy of the resulting tree health mapping. With high resolution multispectral remote sensing data collected in the summers of 2003 and 2004, NDVI was calculated and used to classify each pixel as vegetation or non-vegetation. The pixels representing trees and shrubs were manually selected and extracted, resulting in NDVI data just for trees and shrubs. The remaining data was split into 5 separate layers based on physiognomic tree type (broadleaf deciduous, broadleaf evergreen, conifer, palm, and mixed). Tree health was evaluated at both a pixel scale, and a tree scale, with the pixels or trees being mapped as either healthy or unhealthy. A tree was labeled as unhealthy if 30% or more of the pixels within the manually delineated tree crown were mapped as unhealthy, and if the average NDVI of the pixels were less than the NDVI threshold for healthy trees. The accuracy of the tree health assessment was checked against the validation dataset of 1,186 trees. The field health assessment agreed with the remotely sensed health classification for 88% of the trees.

Fang et al. (2020) used a similar approach to evaluate the health of street trees in Washington D.C. using multispectral remote sensing data and D.C.’s street tree inventory. The tree inventory contained 18,434 trees, each with a tree health classification of excellent, good, fair, poor, or dead. The researchers purchased remote sensing images for June 11, July 30, and August 30, 2017, to compare the sensitivity of tree health at different points in the trees’ on-leaf period. To extract pixels belonging to tree crowns, a radial buffer based on tree crown diameter was used, and pixels

with low NDVI values were masked. This paper tested 5 different vegetation indices (VIs), which included three different variations of NDVI. The different VIs were calculated for each pixel and averaged for each tree. They found that the VI values of trees in good, fair, and poor health conditions were highly statistically different, and traditional NDVI was the most sensitive VI for detecting tree health conditions. Additionally, it was determined that remote sensing imagery taken in the middle of the on-leaf period had the best potential to assess the health condition of trees.

These two studies form the basis of the approach and methods for this thesis, but there are two main places where I believe I can add new insights and improve methodology. First, a frustrating drawback of both Fang et al. (2020) and Xiao et al. (2005) is that a true replication of their process is inaccessible due to the sources of their data. Xiao et al. (2005) used multispectral data that was specially collected just for the UC Davis campus, and Fang et al. (2020) purchased the high resolution multispectral data that was used in their study. Second, there is little consistency in the methods used to select image pixels for NDVI evaluation. Xiao et al. (2005) manually detected and delineated tree crowns for health assessment, and any trees with overlapping crowns were removed from the analysis. Manual crown delineation is extremely time intensive and is an unrealistic method for large sample sizes. In Fang et al. (2020), a standardized radius based on the average DBH of all trees was used to select the tree crown area. However, this method will only use the center pixels of large trees eliminating the edges, and it is unclear how overlapping tree crowns were dealt with. The impact of these different methods on health analysis is unknown.

1.7 The Accessibility of Science

On July 16, 2020, twitter user @GrumpyReviewer2 (2020) shared a screenshot of Nature's posting of an article titled "The growing inaccessibility of science." This article, ironically, was behind a pay wall (Figure 1.1). While this example is ironic and humorous, it highlights a much larger and more serious issue: people are becoming increasingly disconnected from science. This denial or rejection of scientific findings can be seen in the 139 members of the 117th Congress who deny the reality of global climate change (Drennen 2020). Beyond the elected officials, many members of the American public are skeptical of the scientific claims regarding climate change because in some cases, they are not impacted first hand (Markman 2018). People conceptualize things that are psychologically distant from them (in time, space, or social distance) more abstractly than things that are psychologically close (Trope et

al. 2010). Given the relevance of this theory to climate change and the public's disconnect with science, it is important to increase the applicability and accessibility of science and scientific findings. If research remains unattainable for members of the general public, it cannot be expected of them to seek out scientific information and findings. Additionally, if the science that is being done is not relevant to their everyday lives, it may be difficult to give them a reason to care. There is nothing more close to home than one's own backyard, or directly in front of their house. An aspect of science that city residents interact with every day, consciously or not, is the urban forest. By promoting research on urban forests, making the research accessible and relevant, as well as emphasizing the importance of urban forests and urban trees to those who it most directly impacts, we have the opportunity to conduct necessary and beneficial research on urban tree health as well as work to close the psychological gap between people and science.

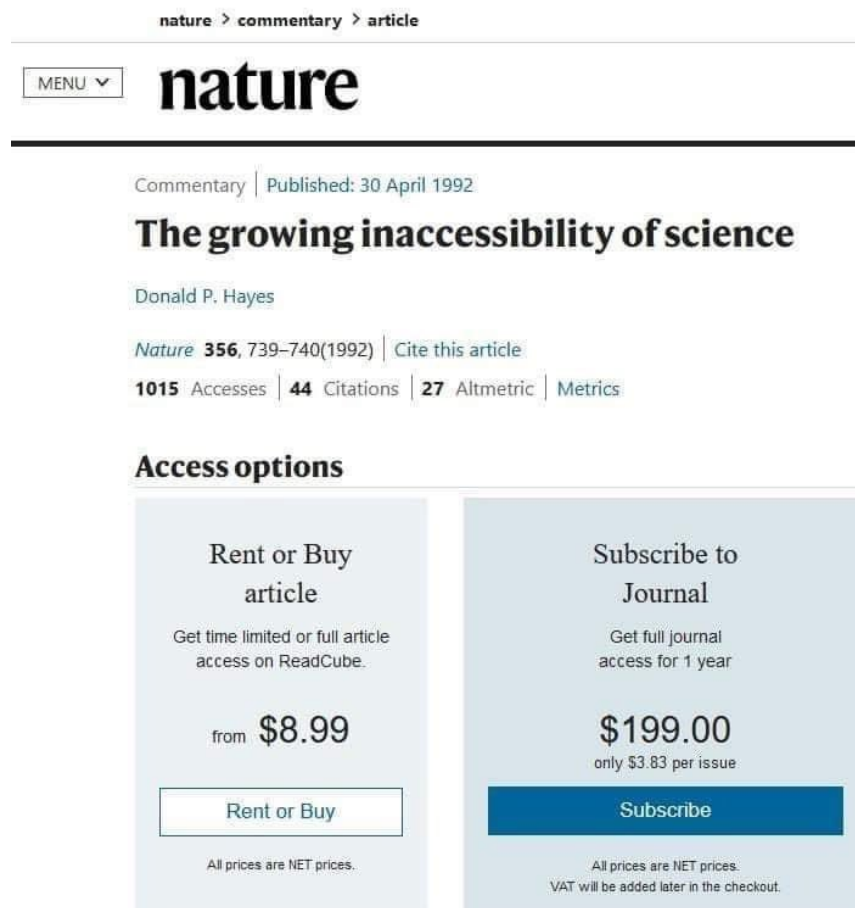


Figure 1.1: The growing inaccessibility of science. Screenshot of Nature website posted on twitter by user @grumpyreviewer on July 16, 2020

1.8 This Thesis

Based on the assumptions that tree health can be approximated using satellite spectral data, specifically NDVI, this thesis aims to build on the process and research of Fang et al. (2020) and Xiao et al. (2005). I will investigate the questions of the impact of species differentiation when using NDVI to calculate tree health, as well as testing three different methods of tree crown delineation and pixel selection. Based on these questions, I predict that differentiating health rating predictions by tree species will improve the accuracy of the model, and differentiating by tree type (coniferous evergreen vs broadleaf deciduous trees) will also improve the accuracy, but less than species. Additionally, I predict that using more in-depth tree crown delineation approaches will allow for more trees to be analyzed, and will also improve the accuracy of the health rating. Finally, this thesis only uses data sources, tools, and processes that are either publicly accessible or free, in order to keep this type of research accessible to all.

Chapter 2

Data Resources and Methods

For this thesis, the data resources and processing components can be split into four main sections (Figure 2.1). First, there is the tree data which is used to answer the question “Where are the trees?” This includes the Portland park and street tree databases, and the subset of those trees that were selected for health data collection and assessment as part of the larger CNH (Coupled Natural-Human) project in the summer of 2021. In this thesis, the tree data is used for tree location points as well as basic tree metrics such as species, height, and crown width. In general, I will refer to these data sources as park trees (the Portland park tree dataset), street trees (the Portland street tree dataset), and CNH trees, which are the trees we collected data on in the summer of 2021. A majority of the processing with the tree points involved tidying and wrangling the data as well as sub-setting it and transforming it into usable data products. Due to the inconsistency in the types of variables measured for each tree data product, I created a model to predict tree crown width and tree height based on DBH and species.

The second aspect of my data and processing is the retrieval and processing of PlanetScope satellite imagery products to produce usable NDVI data files, which was done in Python. Third, are the different tree delineation methods I examine in this thesis, which include point value, radius, and LiDAR methods. This involved the processing of LiDAR and tree crown radius data, as well as obtaining and computing associated NDVI values. Lastly, with the combined data from the previous three parts, I created a predictive model for predicting tree health rating based on NDVI values.

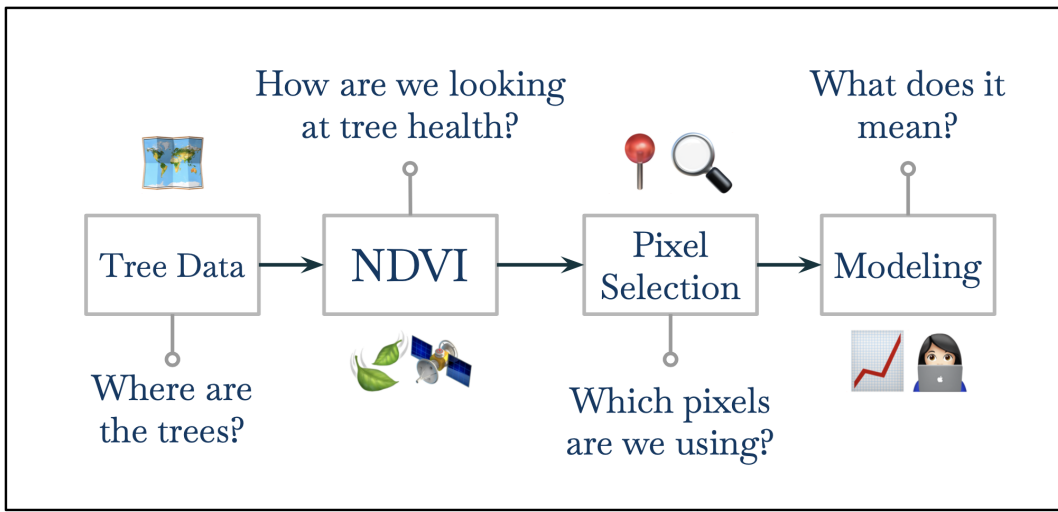


Figure 2.1: Overview of methods and data process

2.1 Previously Collected Field Data

As part of a team of researchers, I collected data tree health during the summer of 2021 as part of the CNH2 Project, which is a larger collaborative interdisciplinary project examining the relationship between various socioeconomic variables and urban tree health (“Smart Trees Collaboratory” 2022).

For the purposes of the larger project, we selected trees from eight different neighborhoods in Portland, with four different categorizations of historic and current investment or disinvestment. The four chosen species are *Pseudotsuga menziesii*, *Pinaceae* (PSME), *Thuja plicata*, *Cupressaceae* (THPL), *Acer macrophyllum*, *Sapindaceae* (ACMA), and *Acer platanoides*, *Sapindaceae* (ACPL). They are some of the most abundant tree species in Portland, and make up a large proportion of Portland’s urban forest. PSME, THPL, and ACMA are all native to the area, whereas Norway Maple is a nonnative tree species that was frequently planted in residential areas, and is now the most common street tree in Portland.

Individual trees for sampling were selected from the Portland tree inventories, with the goal of sampling an equal proportion of street trees and park trees of each species in each neighborhood. Sampling was also focused on mature trees, so the inventories were filtered to only include individuals above 25 feet in height. 4 trees of each species were randomly selected per neighborhood, with an attempt to maintain equal proportions of park and street trees. However, due to varying field conditions, some trees were not able to be sampled, so the nearest tree of the same species that

Table 2.1: Counts of species for final CNH tree dataset

| Common name | Scientific name | Species code | Number collected |
|------------------|----------------------------------|--------------|------------------|
| Bigleaf Maple | * <i>Acer macrophyllum</i> * | ACMA | 29 |
| Norway Maple | * <i>Acer platanoides</i> * | ACPL | 30 |
| Douglas Fir | * <i>Pseudotsuga menziesii</i> * | PSME | 25 |
| Western Redcedar | * <i>Thuja plicata</i> * | THPL | 28 |

met all criteria was substituted. In total, 128 trees were surveyed. Fieldwork was conducted between July 7 and August 19, 2021 (Figure 2.2). Each tree was sampled in a single visit between 10am and 3pm. Biotic and abiotic variables were measured, as well as health attributes and physiology of the trees (Table A.1). For each tree, a GPS point was collected to mark its location using ArcGIS Explorer on IOS. Due to the uncertainty of the GPS points, during post-processing, each collected tree was matched with the tree location point in the Portland Park and Street Tree inventories. Any sampled tree points that did not match up with an inventoried tree point in a margin of 20 feet, it was removed from further analysis. Any tree individual that did not contain a health categorization was also removed. The final CNH dataset for my analysis contained 112 trees (Table 2.1).

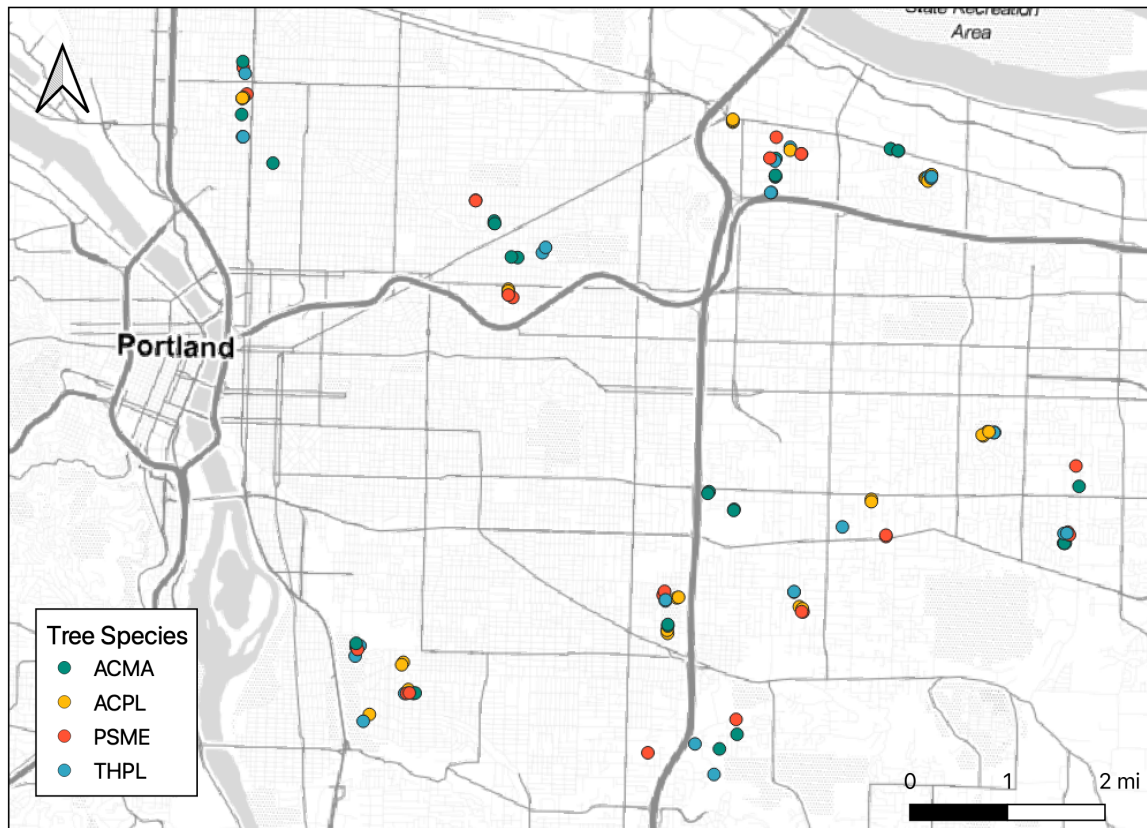


Figure 2.2: Sampled CNH Trees

2.2 Portland Tree Inventory

The Portland Tree Inventory Project, managed by the City of Portland's Parks & Recreation Urban Forestry Department, cataloged nearly 245,000 street and park trees in Portland between 2010 to 2019. The street tree inventory, which was collected from 2010 to 2016, contains information on 216,750 street trees of 145 genera. The park tree inventory, collected from 2017 to 2019, contains data on 25,740 park trees of 116 genera. While many of the collected variables differ between the two inventories, they both include data on location, tree identification, tree diameter at breast height (DBH), and a visual assessment of the trees health which was rated as **good**, **fair**, **poor**, or **dead** (Table A.1).

To reduce the variability in data due to the time span of data collection, I filtered the street inventory to trees collected in 2016, and the park tree inventory to trees that were sampled in 2019. For each dataset, the selected year was the year with the highest count of trees sampled, and the trees from 2016 and 2019 were used in my NDVI analysis and final predictions (Tables 2.2 and 2.3) (McConville 2020).

Table 2.2: Species counts in the Portland Street Trees Database

| Species code | Collected in 2016 | Total in inventory |
|--------------|-------------------|--------------------|
| ACPL | 4373 | 19209 |
| THPL | 578 | 1341 |
| ACMA | 1306 | 2609 |
| PSME | 1254 | 3141 |

Table 2.3: Species counts in the Portland Park Trees Database

| Species code | Collected in 2019 | Total in inventory |
|--------------|-------------------|--------------------|
| ACPL | 411 | 1502 |
| THPL | 331 | 964 |
| PSME | 3237 | 6783 |
| ACMA | 256 | 490 |

The Portland park and street tree inventories include a health categorization variable of **good**, **fair**, **poor**, or **Dead**. A drawback that can come with qualitative health ratings such as this one is that if a tree does not appear close to death, or perfectly healthy, it is very easy to categorize its health as **fair**, which is what we see in both the street and park tree databases. The proportion of trees rated **fair** is extremely high, especially in the park trees inventory (Figure 2.3).

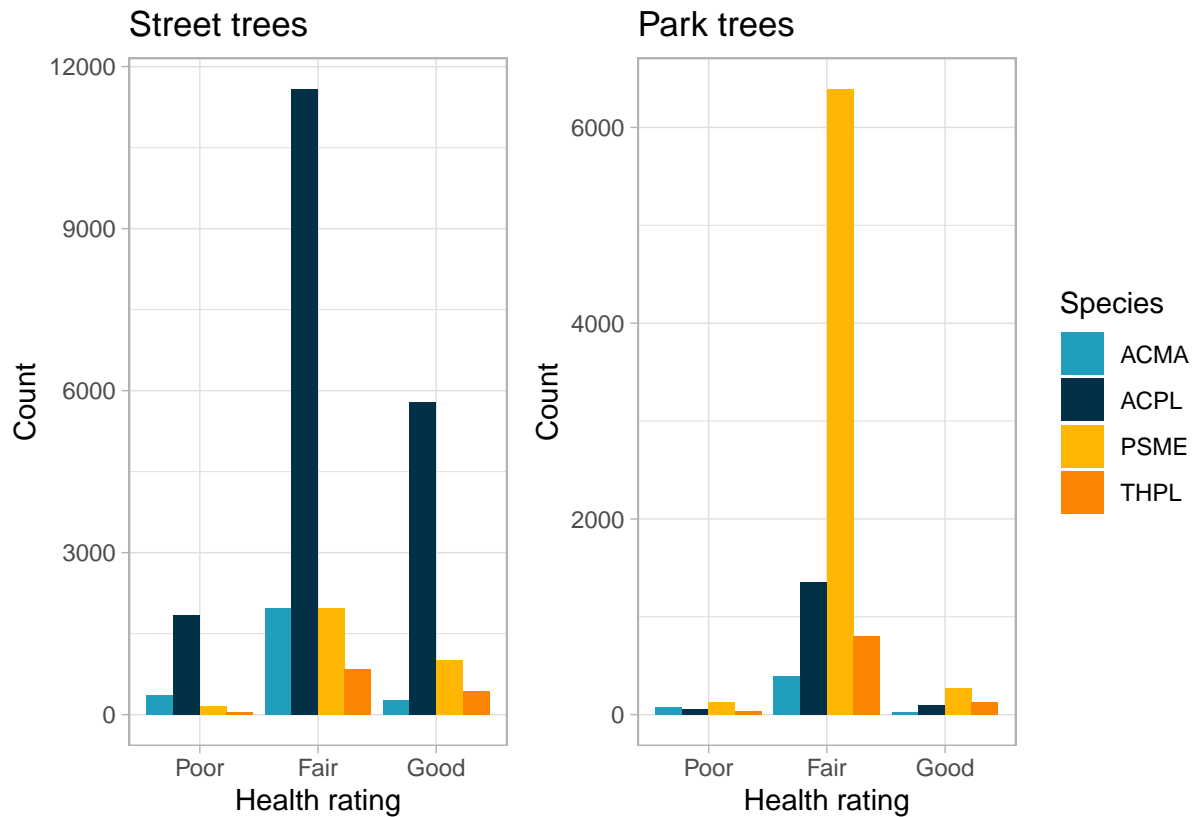


Figure 2.3: Distribution of Health Ratings in the Portland Tree Inventories

2.2.1 Canopy width and tree height model

The park tree dataset contains measurements for tree height, canopy width, and DBH, but the street tree dataset only contains measurements for DBH. In order to successfully filter out all trees shorter than 25 feet tall, a height measurement is necessary. Canopy width is an essential factor of the radius pixel selection method, which is discussed below (section 2.6.2). Using RStudio, I created a statistical model to predict tree height and crown width based on tree DBH and species in order to be able to use the same pixel selection methods for both the park and street tree inventories (section 3.1).

2.3 Satellite Imagery

The multispectral satellite imagery used in this thesis was accessed through Planet Labs Education and Research Program, which provides limited non-commercial access

to PlanetScope satellite imagery for those with a college or university email address. The available imagery had a pixel resolution of 3 meters, and a 4-band product (RGB-NIR). The bands in a satellite product refer to the reflectance wavelength that is picked up by the satellite. For a 4-band satellite product, the wavelengths are split into red, green, blue, and near-infrared (NIR) bands (Table 2.4). In the raw PlanetScope product, these 4 bands come compressed in one .tif image.

Table 2.4: Wavelength ranges for 4-band Planetscope satellite bands

| Band name | Wavelength range |
|-----------|------------------|
| Blue | 455 - 515 nm |
| Green | 500 - 590 nm |
| Red | 590 - 670 nm |
| NIR | 780 - 860 nm |

PlanetScope satellite imagery (Planet Labs, 3m resolution, 4-band RGB-NIR) was used for vegetation index calculation. PlanetScope, also known as the Flock, is a constellation of approximately 130 satellites . The first 28 PlanetScope satellites were launched in July 2014, and the newest batch of satellites were launched in January 2022. PlanetScope, operated by Planet, is a constellation of approximately 130 satellites, able to image the entire land surface of the Earth every day (a daily collection capacity of 200 million km²/day). PlanetScope images are approximately 3 meters per pixel resolution (“Planet Imagery Product Specifications” 2022). A downloaded satellite product for an area of interest is comprised of multiple scene products. Each scene product is an individual image of a swath of land that is at least partially contained within the area of interest. (Figures A.2, A.3, A.4).

I downloaded satellite images corresponding to the summers of when the data was collected (2016, 2019, and 2021). Images were first filtered for those captured in July of each year, since images taken during the middle of the on-leaf period have been shown to be most sensitive in detecting a statistical difference in tree health measured by NDVI (Fang et al. 2020). The remaining images were then filtered for minimal cloud cover and maximum coverage of the area of study. The final selected images were taken between 6:30 and 7pm on 6 July 2016, 31 July 2019, and 26 July 2021 (Table 2.5).

Table 2.5: Satellite product specifications for PlanetScope multispectral satellite image products

| Collection date | Collection time | Number of scene products | Satellite ID |
|-----------------|-----------------|--------------------------|--------------|
| 2016-07-06 | 18:55 | 5 | 0c22 |
| 2019-07-31 | 18:42 | 4 | 0f42 |
| 2021-07-26 | 18:40 | 4 | 1003 |

For each of the chosen dates, I downloaded the available analytic product from Planet. The analytic multispectral imagery products are orthorectified, calibrated, corrected for terrain distortions, and transformed to Top of Atmosphere radiance to ensure accurate geolocation and cartographic projection.

2.4 NDVI calculation

The NDVI calculations were done using Python in PyCharm. Besides minor alterations, the processing code came from Planet's instructions on calculating NDVI from 4-band PlanetScope data (Planet, n.d.). NDVI is calculated from the red and NIR satellite bands, as shown in Equation (2.1). NDVI is calculated for each individual pixel of the satellite image.

$$\text{NDVI} = \frac{(NIR - Red)}{(NIR + Red)} \quad (2.1)$$



Figure 2.4: Product areas for 2016, 2019, and 2021 satellite scenes

2.5 Canopy Height Model

A canopy height model for the Portland metro area was developed using LiDAR and satellite spectral imagery collected in the summer of 2014 (“Canopy 2014” 2016). The purpose of this data is to monitor natural areas in the Portland metro area, specifically change over time analysis and the examination of the potential loss of habitat in riparian areas. The canopy was detected using both NDVI values and LiDAR feature heights. Errors and noise in the data, such as electrical lines above tree tops, were cleaned using geometric post-processing. The canopy height model was clipped to remove anything below ten feet to eliminate any understory shrubs or grasses that were included in the raw data (“Canopy 2014” 2016).

2.6 Tree Crown Delineation and Pixel Selection

The goal of tree crown delineation is to understand where the foliage of a tree is located. This is extremely important because we want to ensure that the satellite pixels used for health analysis have measurements that belong to the given tree. Previous papers such as have used manual tree crown delineation (Xiao et al. 2005), or chosen a standardized radius for all trees in their sample (Fang et al. 2020). Manual tree crown delineation would be extremely time consuming, especially when trying to examine data on a city-wide level. Additionally, with a standardized radius, there will be many trees that have crowns either larger or smaller than the standardized radius. If the true crown is smaller than that of the radius, pixels that correspond to things like grass or pavement will be included in the measurement analysis. Conversely, if the true crown is larger than the chosen radius, the edges of the tree will be ignored, and valuable data will be lost. With both of these methods, any overlapping tree crowns were removed from the final analysis, even further reducing the sample size.

In this thesis, I test three different methods of pixel selection for NDVI analysis. First, I test a “point method” which uses the NDVI value from a single pixel directly below an inventoried trees location point. Second, I use crown width measurements and predictions to create a variable radius method, and average the NDVI pixels within the created circle. Lastly, I use a LiDAR created canopy height model for Portland’s urban canopy with `ForestTools` canopy delineation algorithm to create canopy polygons for NDVI analysis (Plowright et al. 2021).

For the following examples, I use Berkeley Park, located in SE Portland, to demonstrate the different delineation techniques. We sampled 6 CNH trees in Berkeley Park:

2 Bigleaf Maple, 1 Norway Maple, 2 Douglas Fir, and 1 Western Redcedar (Figure 2.5).



Figure 2.5: Berkeley Park and CNH trees

2.6.1 Point method

Point Method: For the point method, I extracted the NDVI value from the pixel directly underneath the tree location point. This is the simplest of the three methods, since it obtains one NDVI value for one singular pixel. The tree location points were sourced from the street and park tree inventories and processed in QGIS (Figure 2.6). The main source of potential error with this technique is with the tree point location. If the point was placed incorrectly, the NDVI value will not be representative of the tree's greenness, or health.



Figure 2.6: CNH trees sampled in Berkeley Park

2.6.2 Radius method

The first method of tree crown delineation I used is based on the individual crown width for each selected tree. In the Portland park tree inventory, crown width is measured as an east to west diameter, and a north to south diameter. To get the radius for the buffer, I took the average of both measurements and divided it by 2. For the Portland street tree inventory, crown width was not collected. I used the tree height and crown width predictive model to create crown width measurements. For each selected tree point, I created a buffer with the radius of the measured or predicted tree canopy using QGIS (Figure 2.7). To get NDVI for each tree in this method, I averaged the value of all pixels in the buffer circle for each tree using QGIS.

With the radius method, it involves the same risk as the point method that if the central point is incorrectly located, the values will not be representative. Additionally, average NDVI ratings obtained with this method for trees with overlapping crowns will contain NDVI pixels that belong to other trees. Previous studies have removed all overlapping tree crowns when using a radius technique, but that can severely limit sample size of available data for analysis, since especially in urban areas and on streets, most of the trees will have overlapping crowns.

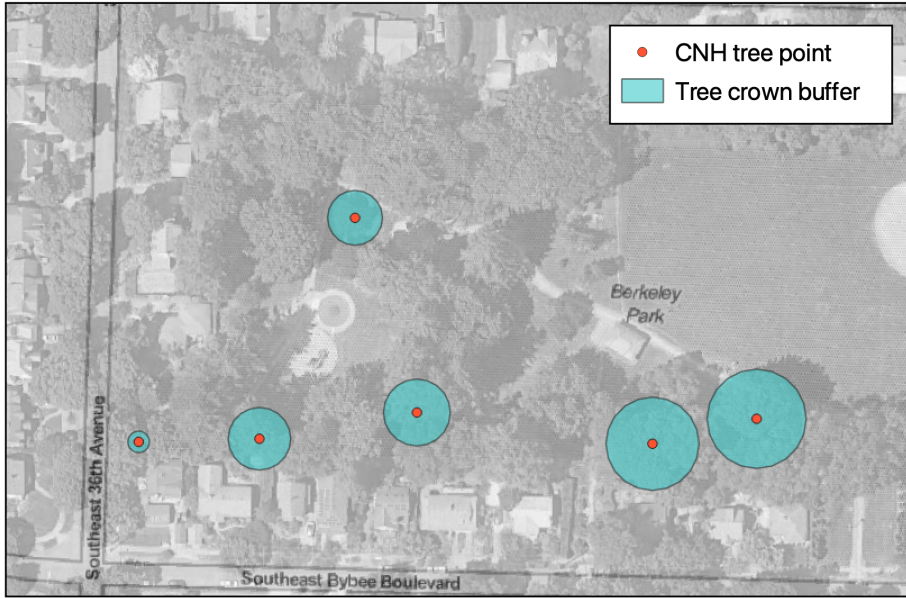


Figure 2.7: CNH trees with crown width buffer

2.6.3 LiDAR method

The LiDAR method is the most complex and involved of the three tree crown delineation methods but has the potential to be the most precise.

The `ForestTools` crown delineation algorithm is a modified watershed delineation algorithm that takes a LiDAR file input, as well as treetop location point file and outputs a polygon file with predicted tree crowns. `ForestTools` also has the ability to predict treetop location points based on LiDAR data, but that functionality introduced a lot of error in my processing because it became difficult to re-associate predicted treetop points with the actual tree location points that I was analyzing.

The LiDAR canopy height model was clipped to a 30 meter buffer around each selected tree point to reduce file size in the delineation processing (Figure 2.8). A 30m buffer was chosen to ensure that no part of the tree canopy would be omitted from the processing, and to include any near neighboring trees that may have canopy that overlaps with the tree of interest. In order for the algorithm to delineate tree crowns, it needs both LiDAR canopy data and location points for the potential trees for delineation. With a smaller buffer radius, the locations of neighboring trees would be omitted and the canopy delineation algorithm would compute a tree crown as much bigger than it actually is.

With the 30m buffer, all other inventoried trees that are contained within the buffer were selected for inclusion as treetop location points in addition to the trees of

interest (Figure 2.9). A minimum tree height of 20 feet was included in the algorithm options but since all sampled trees were already filtered for height requirements, this may not be necessary.

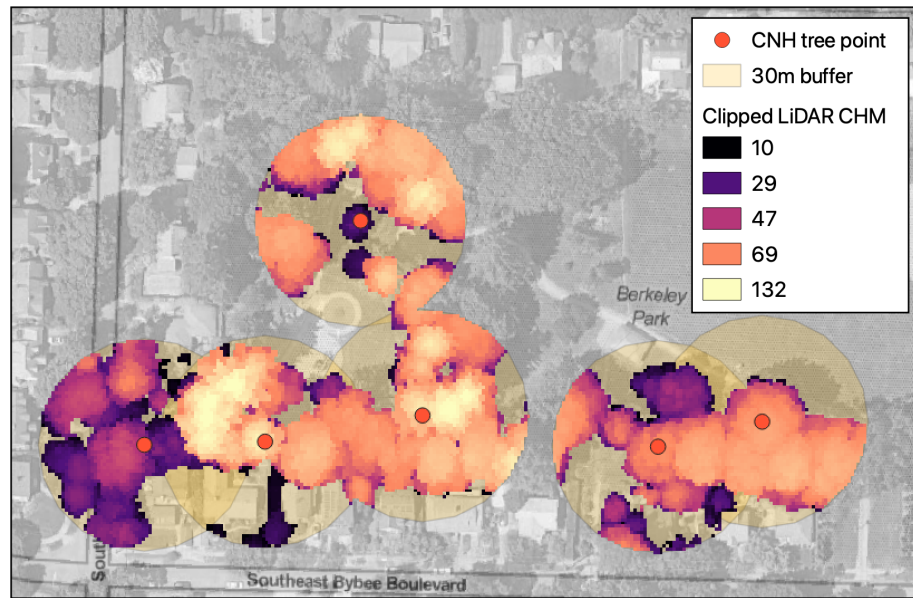


Figure 2.8: LiDAR data clipped to 30m tree buffer

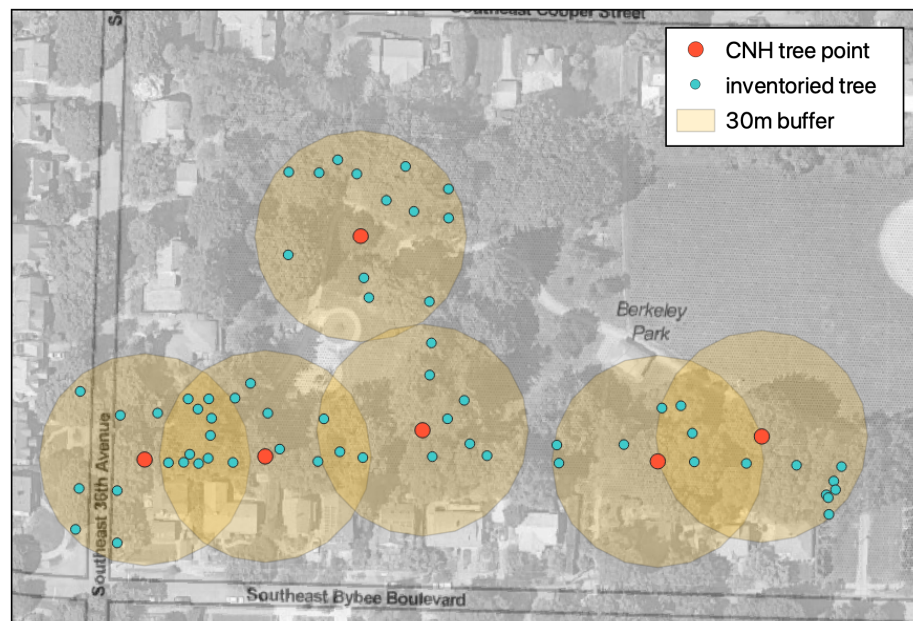


Figure 2.9: All inventoried trees within the 30m buffer

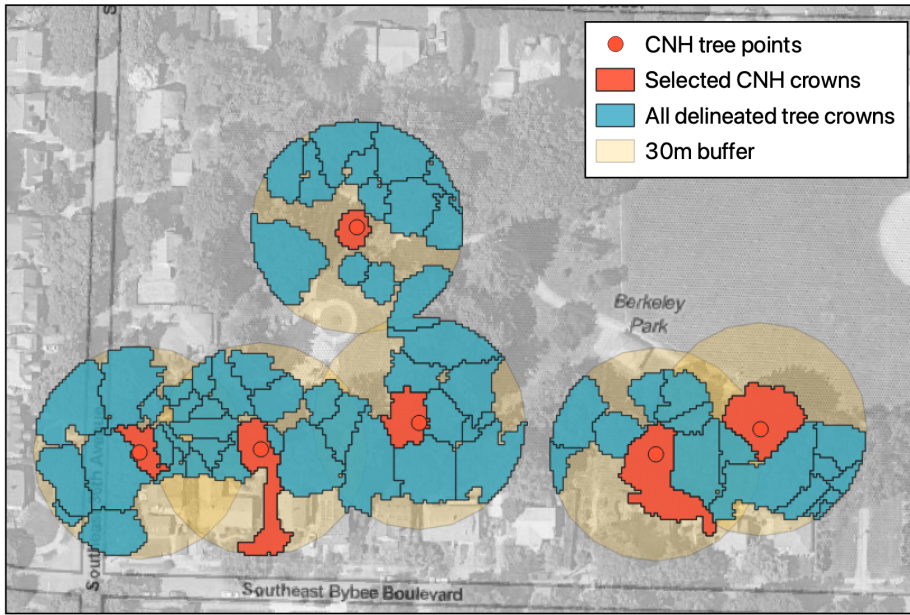


Figure 2.10: LiDAR tree crown delineations with selected CNH crowns

```
include_graphics("figure/layered_outputs.png")
```

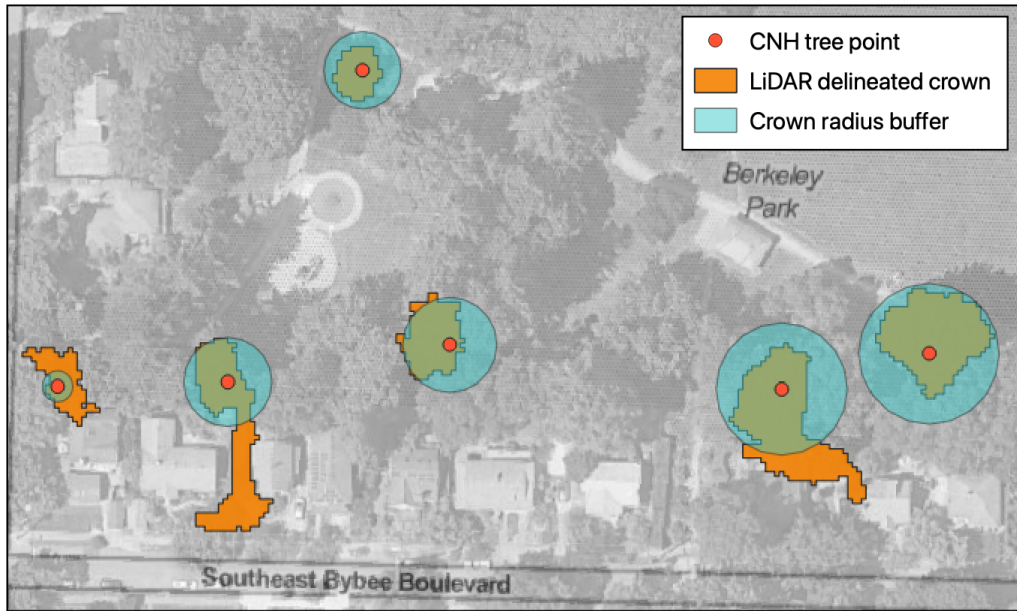


Figure 2.11: Point, Radius, and LiDAR pixel selection methods for Berkeley Park

These three processes were repeated for random samples of 100 park trees and 100 street trees, stratified for tree species. Due to restrictions in file size for LiDAR

processing, the sampling had to be constrained to an area of East Portland (Figure 2.12). This extent was chosen to align with the sampling region of the CNH data, though it had to be shrunk slightly.

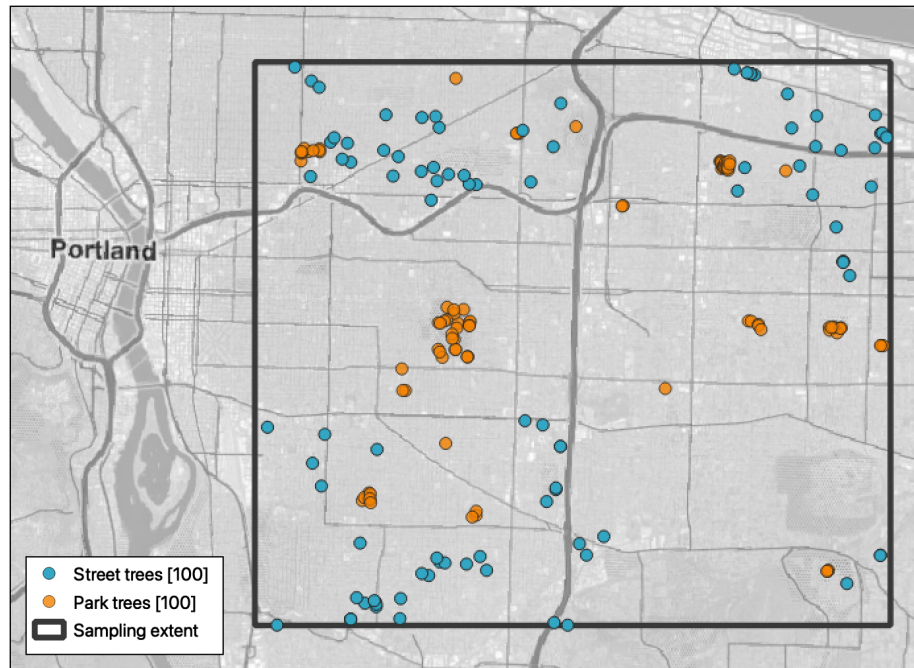


Figure 2.12: Geographic extent and random sampling

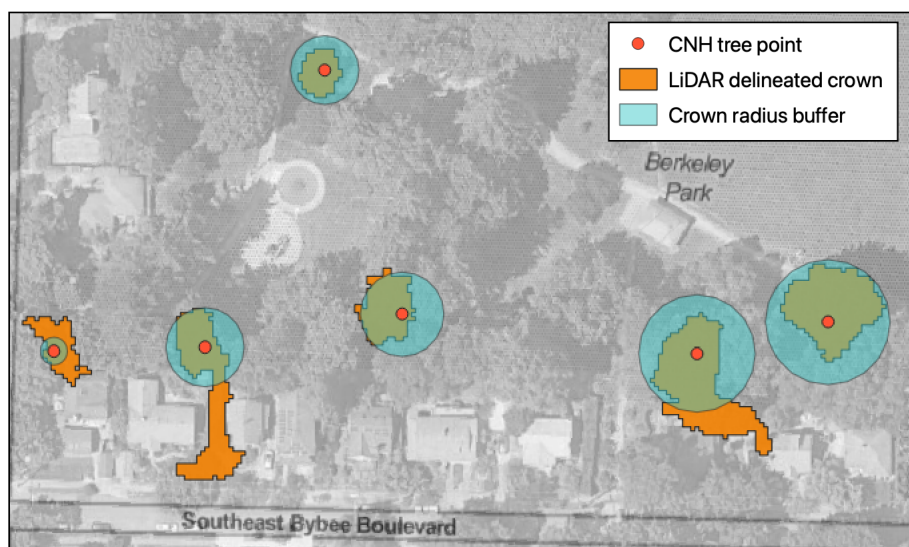


Figure 2.13: LiDAR tree crown delineations with selected CNH crowns

2.7 Modeling Tree Health

To tie all of my smaller pieces of data analysis together, I created a model to predict tree health categorization from NDVI values. I chose an ordinal logistic regression, which is used to model and predict the relationship between an ordinal categorical response variable and one or more explanatory variables, which can be either categorical or continuous. An ordinal logistic regression (OLR) is applicable when there are three or more categories that have a natural and inherent ordering of levels, but the intervals between these levels are not necessarily equal. An OLR model is a modified binary logistic regression model that incorporates the ordinal nature of the dependent variable by defining the probabilities differently. Instead of solely considering the probability of an individual event, an OLR considers the probabilities of that event and all events that are ordered before it (Shi, n.d.; Venables et al. 2002). The function `polr()` within the `MASS` R package is used to fit a logistic regression model to an ordered factor response (Ripley 2021).

In order to use this type of model, I tested each model for the Proportional Odds Assumption which a necessary prerequisite of running an ordinal logistic regression. I used the Brant Test for ordinal logit models which is in the `brant` package (Schlegel et al. 2020; Brant 1990).

For each model, I created a confusion matrix to examine the validity of the model. A confusion matrix is a calculated cross-tabulation of observed and predicted classes, which in this case is health categorization, along with associated statistics. The two main statistics I use in my data analysis are overall accuracy and an un-weighted Kappa statistic. “Accuracy” (2.4) refers to the sensitivity (2.2) and specificity (2.3) of the prediction.

$$\text{Sensitivity} = \frac{\text{True positive}}{\text{True positive} + \text{False negative}} \quad (2.2)$$

$$\text{Specificity} = \frac{\text{True negative}}{\text{True negative} + \text{False positive}} \quad (2.3)$$

$$\text{Accuracy} = \frac{\text{Sensitivity} + \text{Specificity}}{2} \quad (2.4)$$

Kappa (κ) refers to Cohen’s Kappa Statistic which is used to measure inter and intra-rater reliability for categorical items (2.5) (McHugh 2012; Cohen 1960). In this case,

the “raters” are the measured vs predicted health categorizations.

$$\kappa = \frac{p_o - p_e}{1 - p_e} = \frac{1 - p_o}{1 - p_e} \quad (2.5)$$

where p_o is the relative observed agreement between the reference and prediction, and p_e is the hypothetical probability of agreement by chance.

For k categories, N observations to categorize and n_{ki} the number of times rater i predicted category k :

$$p_e = \frac{1}{N^2} \sum n_{k1} n_{k2} \quad (2.6)$$

$$p_e = \sum_k \widehat{p_{k12}} = \sum_k \widehat{p_{k1}} \widehat{p_{k2}} = \sum_k \frac{n_{k1}}{N} \frac{n_{k2}}{N} = \frac{1}{N^2} \sum n_{k1} n_{k2} \quad (2.7)$$

Where $\widehat{p_{k12}}$ is the estimated probability that both raters 1 and 2 will classify the same item as category k , while $\widehat{p_{k1}}$ is the estimated probabilities that rater 1 will classify an item as category k . This is based on the assumption that the rating of the two raters are independent. $\widehat{p_{k1}}$ is estimated from the number of items classified as category k by rater 1 (n_{k1}) divided by the total number of items for classification (N): $\widehat{p_{k1}} = \frac{n_{k1}}{N}$. These equations and relationships are the same for rater 2. If the two raters (in this case the reference and prediction categorizations) are in complete agreement, then $\kappa = 1$.

For each model, I evaluate the success and ability to predict health rating in a few different ways. First, I examine the calculated accuracy and kappa values. A higher kappa value is more important than a higher accuracy score because kappa takes into account the various sizes of the categories and the probability of the prediction occurring by chance, whereas accuracy does not. Additionally, I look at the false positives (a **poor** tree getting rated **good**) and false negatives (a **good** tree being rated **poor**). Both of these values should be as low as possible, but in this case reducing the number of false positives is most important because if a tree in **poor** health was rated as **good**, it may not be included in further health analysis and will be missed when examining the spatial distribution of tree health.

Chapter 3

Results

3.1 Canopy Width and Tree Height Model

I used a second order polynomial regression to predict both tree height and crown width from tree DBH. The tree height predictions were used to filter out trees below 25 feet in height, and the crown width predictions were used in the radius method of pixel selection for NDVI analysis. There are numerous expected differences between the species due to functional tree type. For example, the average DBJ for ACMA and PSME are relatively close, but the average height for a PSME individual is nearly twice as tall as an ACMA (Table 3.1). Because of this, DBH would have a very different effect on the outcome of both models depending on the species of the tree. I included species as an interaction term in the model to account for these expected differences between species, meaning that both DBH and species were used to predict crown width and tree height. I tested a linear model as well as second and third order polynomial models for both predictive models (Figures A.5, A.6). A second order polynomial was chosen for the predictive models because it not only encapsulated the relationship between DBH and tree height as well as DBH and canopy width, but it also was the most accurate when modeling the individual species. When I modeled each species individually for both tree height and canopy width, I got the same results as if I created one model and included species as an interaction term. The tree height model has an adjusted R-squared value of 0.7834, and a P-value of < 2.2e-16 (Figure A.7, Appendix equations (A.1), (A.3), (A.5), (A.7)). This model was most effective for ACMA and PSME, but was not statistically significant for ACPL or THPL. This is likely due to the similar average DBH and tree height values between ACPL and PSME. While the average DBH values for ACMA and PSME are very similar, the average height values are extremely different, with the average

Table 3.1: Average physiological measurements for selected species in the Park Trees database.

| Species | Avg. DBH | Avg. Tree Height | Avg. Crown Width |
|---------|----------|------------------|------------------|
| ACMA | 29.28 | 69.49 | 49.39 |
| ACPL | 20.34 | 49.77 | 44.80 |
| PSME | 29.57 | 112.14 | 39.47 |
| THPL | 18.11 | 50.14 | 24.14 |

PSME individual standing twice as tall as the average ACMA individual (Table 3.1). An issue with the second degree model is the decrease in predicted tree height. This decrease is not seen in the park tree model, but the street tree height predictions for all species show a visible decrease after the inflection point of the model. Given that the tree height predictions were only used for filtering out trees below 25 feet in height, an extremely precise model was not necessary for the purposes of this thesis.

The crown width model has an adjusted R-squared value of 0.7269, and a P-value of $< 2.2\text{e-}16$ (Figure 3.1, Appendix equations (A.2), (A.4), (A.6), (A.8)). The coefficients for the canopy width model had statistically significant p-values for all species. There is consistent variation in the average crown width measurements between all species (Table 3.1). With the visualization of the street tree canopy width predictions, the only extreme decrease after the model inflection point is seen in the ACPL predictions. The canopy width model played a larger role in this thesis than the tree height model because it was essential for the radius method of pixel selection for all street trees.

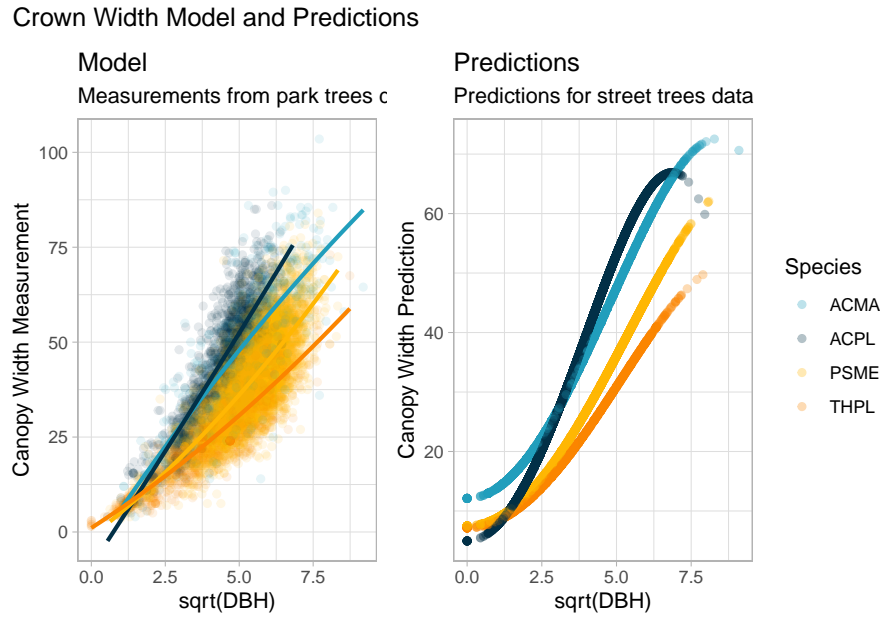


Figure 3.1: Second order polynomial model for predicting tree crown width based on measured DBH and species, with predictions for street trees. ($R^2 = 0.7269$, $P < 2.2e-16$)

3.2 Health Rating vs. Tree Type and Tree Species

For all trees collected as part of the CNH field work, I examined the potential existing relationships between measured health rating and tree functional type, as well as between health rating and tree species. A Chi-Square Test of Independence was performed to assess the relationship between health rating and functional tree type. There was a significant relationship between the two variables ($X^2(2, N=112) = 10.184$, $p = 0.00615$). Within functional tree type, both conifers and broadleaf trees were most likely to be rated as **fair**, but within health category a **good** or a **poor** tree were most likely a broadleaf tree, and a **fair** tree was most likely a conifer (Table 3.2). A Chi-Square Test of Independence was performed to assess the relationship between health rating and tree species. There was a significant relationship between the two variables ($X^2(6, N=112) = 22.368$, $p = 0.00104$). Within tree species, ACMA, PSME, and THPL were all most likely to be rated as **fair**, but ACPL was most likely to be rated as **good**. Within health category, a **poor** tree was most likely an ACMA individual, a **fair** tree was equally likely to be a PSME or THPL individual, and a **good** tree was most likely an ACPL individual (Table 3.5).

Table 3.2: Frequency and probability tables of functional tree type and health rating for CNH trees. There is a statistically significant relationship between the two variables ($X^2(2, N=112) = 10.184$, $p = 0.00615$)

| | broadleaf | conifer |
|------|-----------|---------|
| poor | 9 | 6 |
| fair | 28 | 40 |
| good | 22 | 7 |

| | broadleaf | conifer |
|------|-----------|-----------|
| poor | 0.0803571 | 0.0535714 |
| fair | 0.2500000 | 0.3571429 |
| good | 0.1964286 | 0.0625000 |

Table 3.5: Frequency and probability tables of functional tree type and health rating for CNH trees. There is a statistically significant relationship between the two variables ($X^2(2, N=112) = 10.184$, $p = 0.00615$)

| | ACMA | ACPL | PSME | THPL |
|------|------|------|------|------|
| poor | 7 | 2 | 1 | 5 |
| fair | 16 | 12 | 20 | 20 |
| good | 6 | 16 | 4 | 3 |

| | ACMA | ACPL | PSME | THPL |
|------|-----------|-----------|-----------|-----------|
| poor | 0.0625000 | 0.0178571 | 0.0089286 | 0.0446429 |
| fair | 0.1428571 | 0.1071429 | 0.1785714 | 0.1785714 |
| good | 0.0535714 | 0.1428571 | 0.0357143 | 0.0267857 |

3.3 Health Rating vs. NDVI: Point Method Obtained Data

With the selection of CNH trees and 2021 NDVI data, a statistical analysis of the point value method shows that there is a statistically significant difference in NDVI values between health categorizations of **fair** and **good** (ANOVA, $F_{2,109} = 3.892$, $P = 0.023$, TukeyHSD). There is a general positive correlation between NDVI and health category, specifically **fair** and **good**. The relationship between health and NDVI is more apparent in the two maple species, but still holds in the **fair** and **good** categories in the two coniferous species (Figure 3.2). While the difference between NDVI values and health ratings is statistically significant for the point data as a whole, this is not true for all species. The difference in NDVI between **fair** and **good** rated trees is only statistically significant for THPL, meaning that this statistically significant relationship in the point method data is entirely driven by the THPL measurements (ANOVA: $F_{2,25} = 3.834$, $P = 0.0353$; TukeyHSD: **good-fair** $P = 0.031$). There is no statistical significance when split by functional tree type.

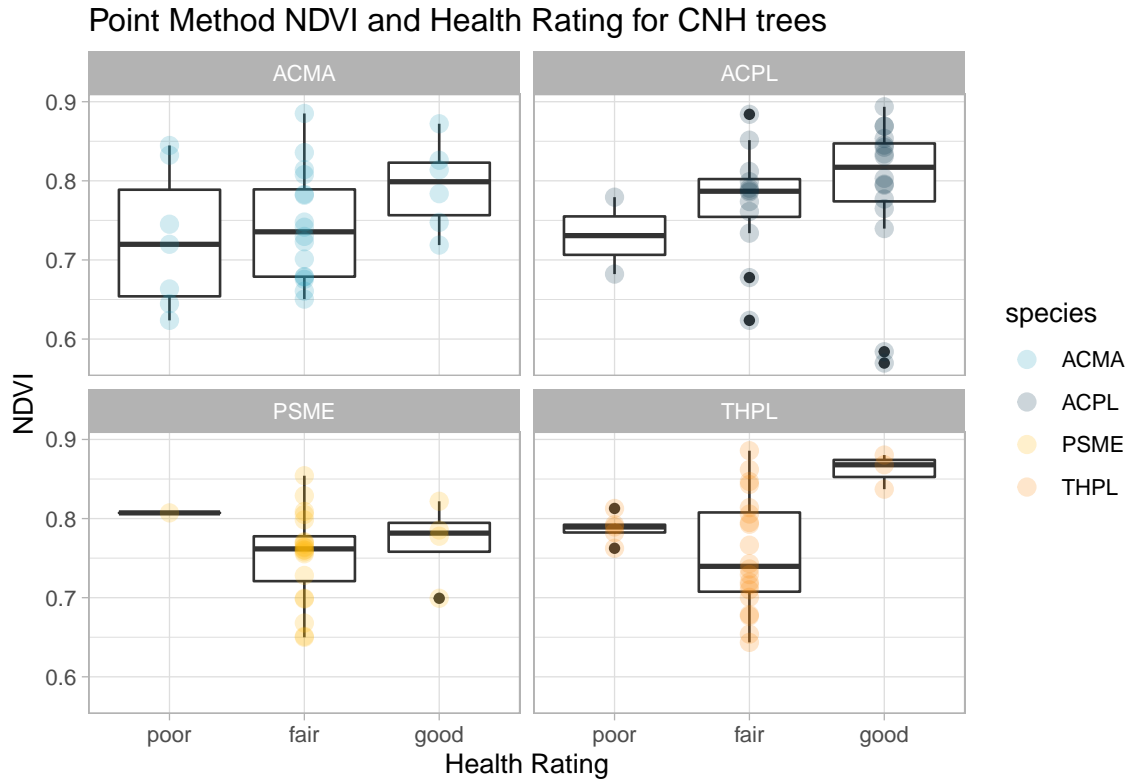


Figure 3.2: NDVI extracted for CNH trees using the point method compared to CNH tree health categorization. There is a statistically significant difference between **fair** and **good** (ANOVA, $F_{2,109} = 3.892$, $P = 0.023$, TukeyHSD)

3.4 Health Rating vs. NDVI: Radius Method Obtained Data

With the radius method of pixel selection and crown delineation, there is a statistically significant difference in the mean NDVI values for health categories (ANOVA, $F_{2,109} = 4.923$, $P = 0.0089$; TukeyHSD: **good-poor** $P = 0.033$, **good-fair** $P = 0.014$). Similar to the point method, there is a larger difference in average NDVI between the **fair** vs **good** categories than **poor** vs **fair**, which is statistically significant in the radius method results (Figure 3.3). When the statistical analysis is split by tree species, there is no statistical significance. When split by functional tree type, there is a statistically significant difference in the NDVI values between **good** and **poor** health ratings for broadleaf trees (ANOVA, $F_{2,56} = 3.976$, $P = 0.0243$, TukeyHSD).

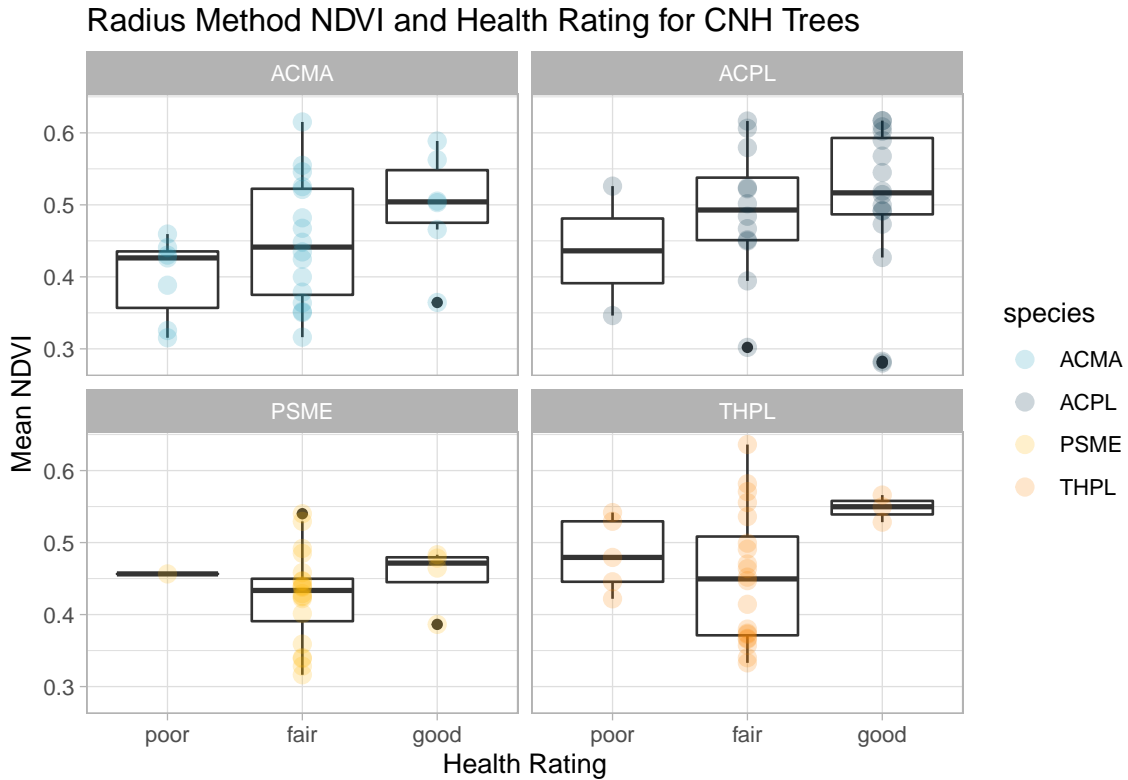


Figure 3.3: Boxplot of average NDVI from radius method and health condition, by species. The relationship between NDVI and health category is strongest in the maples, but still somewhat apparent in the conifers. (ANOVA, $F_{2,109} = 4.923$, $P = 0.0089$; TukeyHSD: good-poor $P = 0.033$, good-fair $P = 0.014$)

3.5 Health Rating vs. NDVI: LiDAR Method Obtained Data

There is a statistically significant difference in NDVI between health categories for the LiDAR method, specifically between **good** and **fair** (ANOVA, $F_{2,101} = 5.405$, $P = 0.00589$, TukeyHSD). The same relationship between NDVI and health condition for the maples that was seen in the point and radius method is seen here (Figure 3.4). Again, when split by species, there is no statistical significance. However, when split by functional tree type there is a statistically significant difference between the average NDVI values for **good** and **poor** health categories for broadleaf trees (ANOVA, $F_{2,51} = 3.498$, $P = 0.0377$, TukeyHSD).

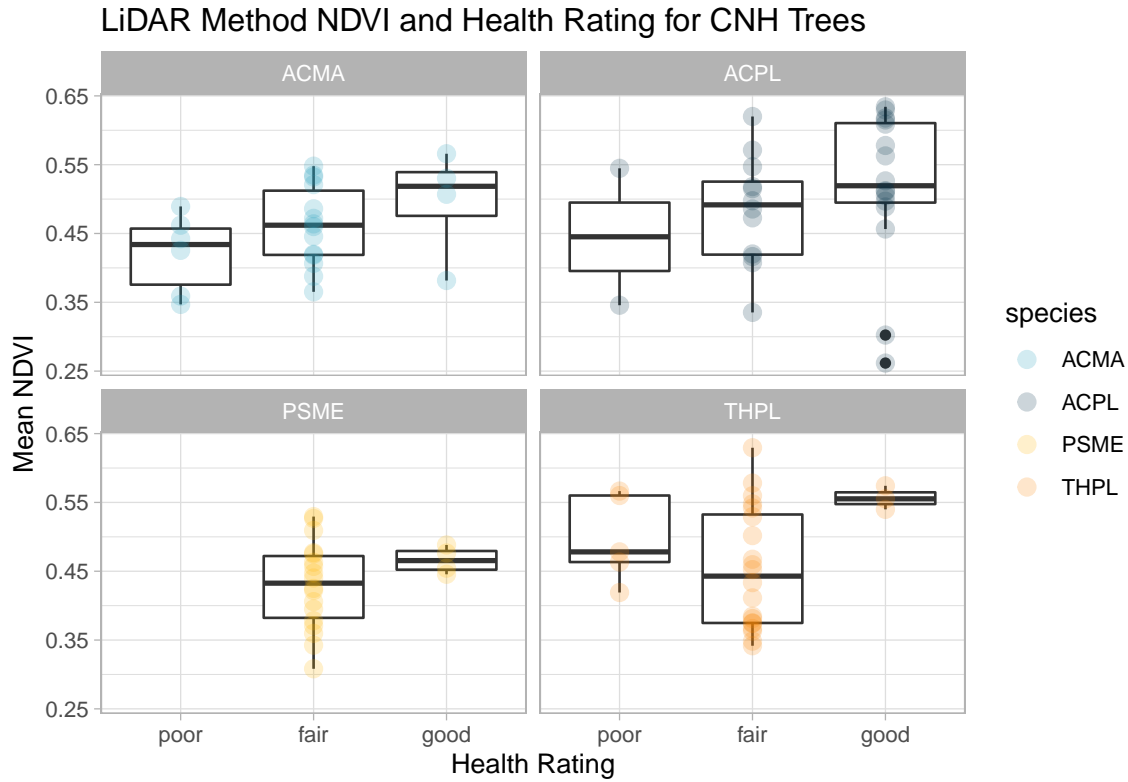


Figure 3.4: Boxplot of average NDVI from LiDAR method and health condition for each species. Due to the nature of the LiDAR delineation algorithm, no crown was detected for the PSME individual with a **poor** health rating. The difference between **good** and **fair** average NDVIs is statistically significant (ANOVA, $F_{2,101} = 5.405$, $P = 0.00589$, TukeyHSD)

Another aspect of the LiDAR delineation method is the potential for data loss. Five ACMA and three PSME individuals were lost in the LiDAR crown delineation process. If this was with a very large sample size the data loss would likely not be detrimental but especially with a sample size such as mine, a loss of eight trees is a loss of 5% of the total data, 17% loss for ACMA, and 12% loss for THPL.

3.6 Method Comparison

There is no statistically significant difference in NDVI values for the three different pixel selection methods, which were standardized to z-scores for NDVI (ANOVA, $F_{2,325} = 0$, $P = 1$). For each method, Z-scores were calculated for the NDVI values. The mean Z-score for point method NDVI for trees rated **poor** is above zero meaning that the raw NDVI value for a **poor** rated tree is higher than the mean average

NDVI value for point method trees. For the radius and LiDAR data, the average z-score for **poor** rated trees is below the mean average NDVI value for each method. Interestingly, the mean z-score for **poor** LiDAR trees is higher than for **fair** trees.

When the species are clumped, the three methods show very similar patterns, though the NDVI values are higher for the point method than either of the other two methods (Figure 3.6). When all three methods are compared along with species, we can see that the general trend of health rating and NDVI is consistent within each species. The pattern between health rating and NDVI is also very similar between trees of the same functional type (Figure 3.6). Because of these similarities in health rating and NDVI values for trees belonging to the same functional type, I included additional testing examining the difference in species specificity addition versus functional type separation.

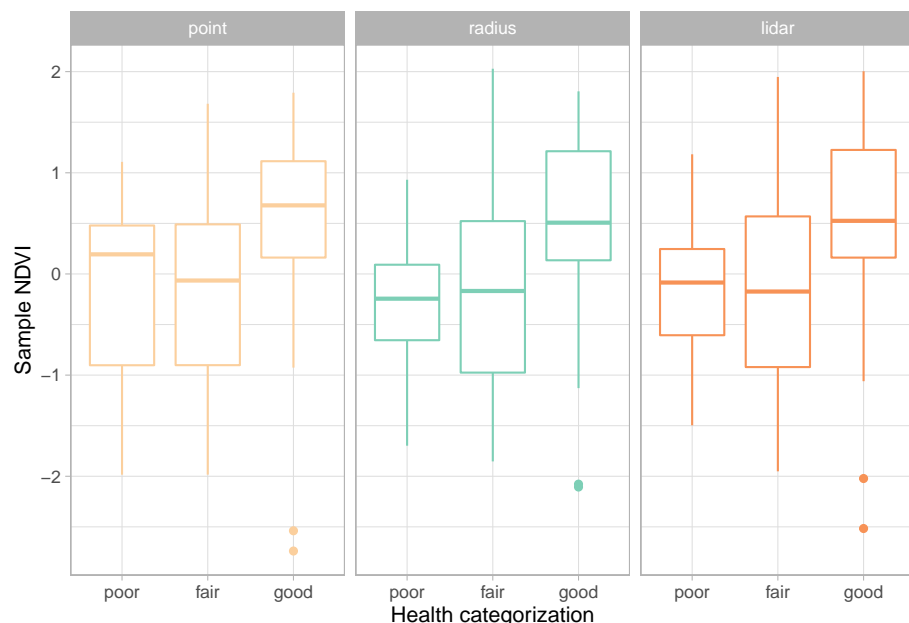


Figure 3.5: Z-score of NDVI values from all three pixel selection methods with CNH health rating. There is no statistically significant difference in NDVI trends between pixel selection methods. (ANOVA, $F_{2,325} = 0, P = 1$)

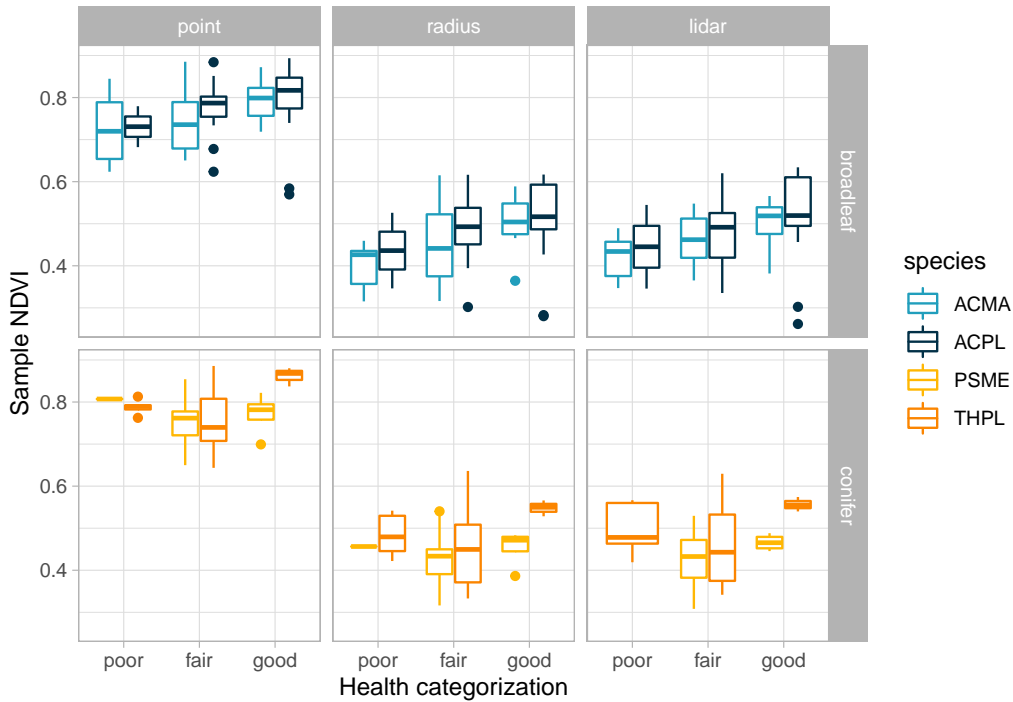


Figure 3.6: Average NDVI for each health category, split by functional tree type and pixel selection method. The general trends remain the same for each individual species, but varies between functional type. The same trends can be seen for trees of the same functional type (broadleaf vs conifer).

Another important factor to consider when comparing the three pixel selection methods is the amount of pixels used in the NDVI analysis. For the point method, each NDVI value is based off one singular point. For both LiDAR and Radius methods, the NDVI used in prediction is an average of all NDVI values captured within the pixel selection method, but the number of pixels used varies between methods and species (Figure 3.7). Each successive model reduced the number of points that are statistical outliers

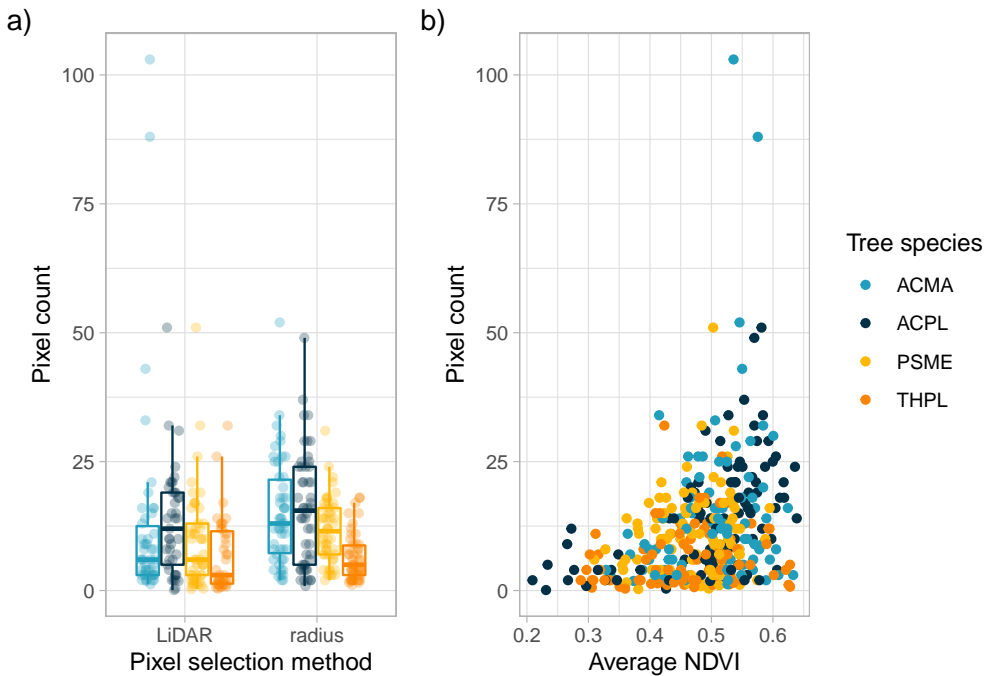


Figure 3.7: Comparison of pixel counts used in NDVI calculations. (a) Boxplot of pixel counts used for each species in the LiDAR and radius methods. For both methods, the maples had more outliers than the conifers, and THPL had the lowest average number of pixels used. (b) Pixel count and average NDVI per tree. There does not seem to be any strong statistical relationship between the number of pixels used and the sample NDVI, though this does not include any data from the point method.

3.7 Predictive Model

I used ordinal logistic regression models with the goal of predicting tree health rating from NDVI. In order to determine the impact of differentiating by species in predictive models, I ran three different models for each point selection method, moving from least to most specific: a model that only uses NDVI to predict health rating, a model that includes functional tree type as an interaction term, and a third model that includes species as an interaction term (Table A.2).

Due to the limited sample size of the data I am working with, the following models are trained and tested on the same data, which is the CNH tree data collected summer 2021. I chose to do this because of the limited sample size of CNH trees, and the uneven size of the health category ratings. Because of this, it is important to note that the model tests are an idealized version of a true model. However, it is important

to note that they are idealized version of how model testing and training would work in reality.

With the point method data, the first model using only NDVI as a predictor (health rating \sim point NDVI) led to all tree points being rated as **fair** (Figure 3.8a). For the continuous variable of NDVI, the coefficient value of 7.041 can be interpreted as that with one unit increase in NDVI, the log of odds of having a **good** health rating increase by 7.041. With the t-value of 2.479, this is statistically significant at the .05 level. The intercept for **poor** vs **fair** shows that the log of odds of a tree being rated as **poor** versus **fair** or **good** is not statistically significant, but the log odds of a tree being rated **poor** or **fair** versus **good** are statistically significant.

The model using tree type as an additional predictor (health rating \sim point NDVI * tree type) had an increase in predictions of **good** health trees, and increased kappa from 0% to 15% (Figure 3.8b). The overall accuracy only increased by 2%, but kappa is more informative in terms of model validity than the accuracy score. With this model, one unit increase in NDVI will lead to an increase in the log odds of having a **good** rating by 10.2 (t-value = 2.685). The impact of a tree being classified as a conifer, versus a broadleaf tree, were not statistically significant at the 0.05 level. Again, the intercept for **poor** vs **fair** is not statistically significant, but the log odds of a tree being rated **poor** or **fair** versus **good** are statistically significant.

Using tree species instead of tree type in the model (health rating \sim point NDVI * species) further improved the kappa of the model. The number of **good** trees that were correctly predicted increased from 7 to 13, but additionally the number of **fair** trees that were correctly predicted dropped from 64 to 59, with the new predictions as **good** (Figure 3.8c). None of the models that used the point method obtained data were able to correctly predict any trees with **poor** health categorization, and in models b and c, each had one **poor** tree that was incorrectly predicted as **good**.

Confusion Matrixes for Point Method NDVI Models

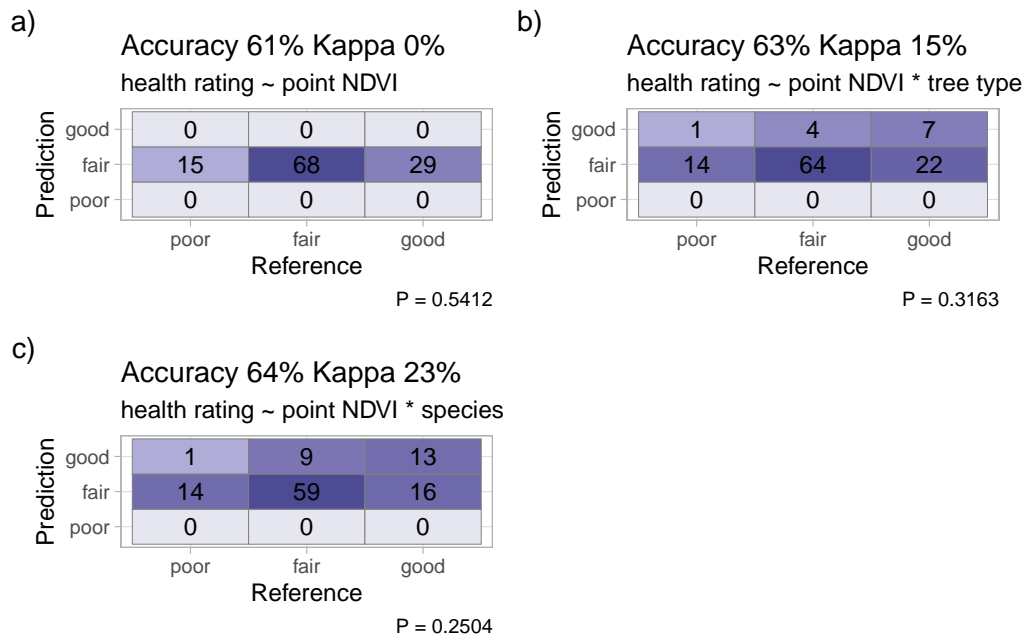


Figure 3.8: Confusion Matrix results for three predictive models, using point method obtained NDVI data to predict three health rating. (a) Model only using NDVI to predict health rating. (b) Model using both NDVI and functional tree type (broadleaf vs confier) to predict health rating. (c) Model using NDVI and tree species to predict health rating.

Using just NDVI as a predictor in the model (health rating ~ radius NDVI) still performs the worst of the three models, with 96% of the sampled trees being predicted as **fair** (Figure 3.9a). Similar to the point method with no interaction term (health rating ~ point NDVI), the **fair** vs **good** intercept is the only one that is statistically significant. However, this model has a t value of 3.68, meaning this model performs better than the point method model with the same formula. When using tree type as predictor variables (health rating ~ radius NDVI * tree type), there was an increase in the number of trees being rated as in **good** health of 9 trees in total, but only 6 of those were additional correct predictions (Figure 3.9b). Again, the intercept of **fair** vs **good** is statistically significant, meaning that the log of odds of a tree in this model being rated **poor** or **fair** versus **good**. The main takeaway from the radius method models is that with the inclusion of species as an interaction term with the radius data (health rating ~ radius NDVI * species), we see our first predictions of the **poor** category. There is no increase in statistical significance of the log odds between the previous model and this one. The radius method does involve more pixels than the

point method, and with the range in NDVI values being lower than that of the point method it makes sense that there is an increase in **poor** rated trees. However, out of the 15 reference trees with health ratings of **poor**, only one was correctly predicted as such (Figure 3.9c).

Confusion Matrixes for Radius Method NDVI Models

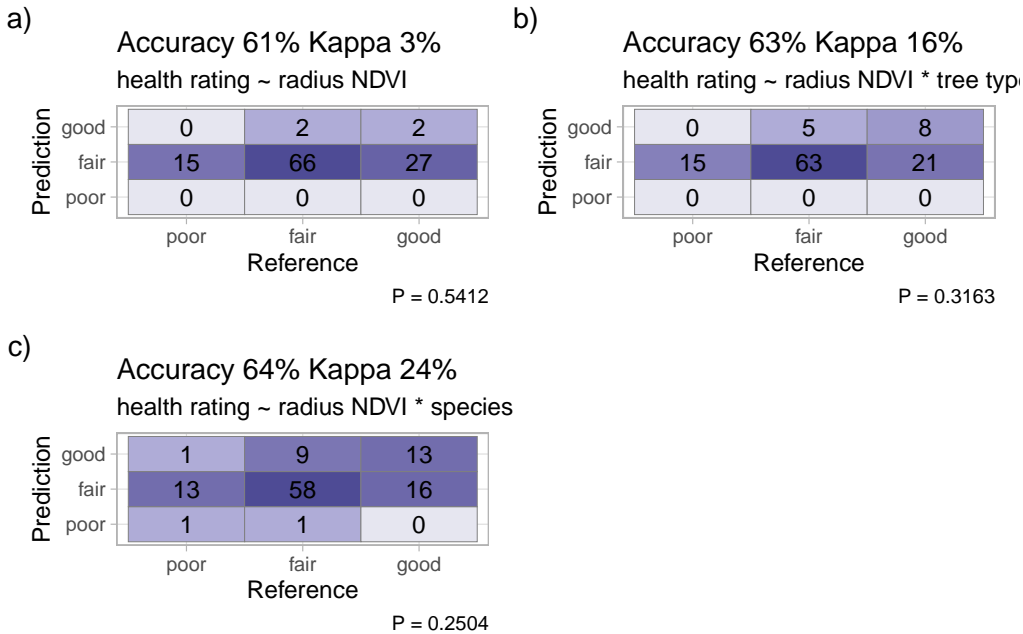


Figure 3.9: Confusion matrixes for each species predictions with radius method data. (a) Model using only NDVI to predict health rating. (b) Model with the addition of functional tree type as a predictor. (c) Model using tree species as a variable when predicting tree health rating.

The LiDAR data was the most effective at predicting tree health across all three pixel selection methods. With the first model using only NDVI to predict health rating (health rating ~ LiDAR NDVI), more trees were correctly predicted as **good** than the same model with the other two methods (Figure 3.10a). With the addition of tree type as a predictor variable (health rating ~ LiDAR NDVI * tree type), the number of correctly predicted **good** trees increased, but most importantly, the number of **fair** trees predicted as **good** remained the same where with the other two methods, that count had increased as well. However, this model also included a **good** tree being predicted as **poor** which no other variations of the models did (Figure 3.10b). The last model with species as an interaction term (health rating ~ ILiDAR NDVI * species) was the most effective of all 9 models, with the highest accuracy and kappa,

as well as the smallest p-value (Figure 3.10c).

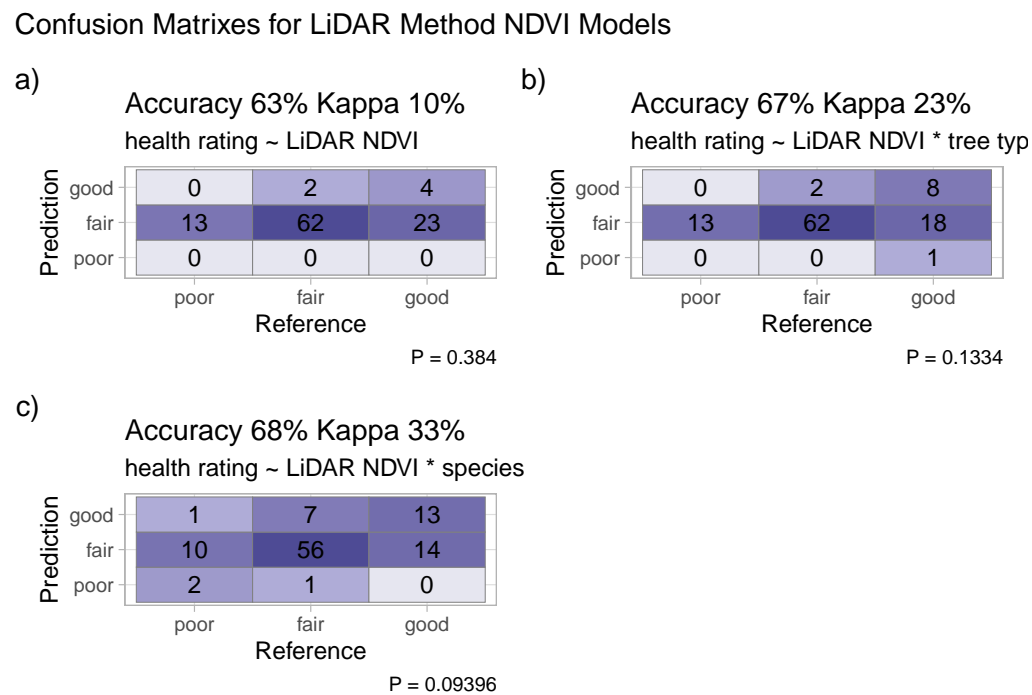


Figure 3.10: Confusion matrixes for each species predictions with LiDAR method obtained NDVI values. (a) Model using NDVI to predict tree health category. (b) Model using functional tree type in addition to NDVI for health prediction. (c) Model with species as a predictor variable for NDVI based tree health category.

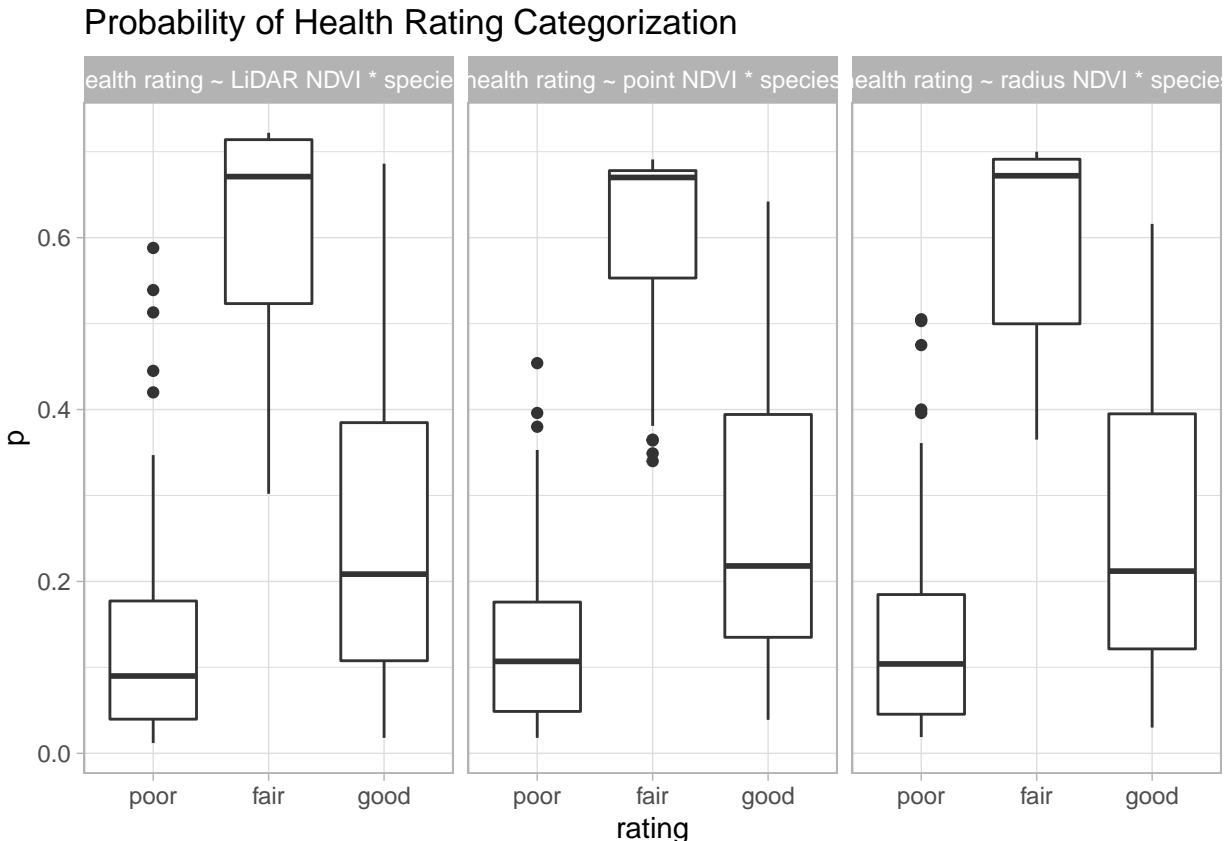


Figure 3.11: Boxplot of probabilities of health group categorization

With the results of the models using species as an interaction term for each of the three pixel selection methods (health rating \sim point NDVI * species; health rating \sim radius NDVI * species; health rating \sim LiDAR NDVI * species), I compared the probabilities of a given tree being assigned each health category (Figure 3.11). For each prediction, a probability of assignment to each health category is created (Table ??). The probability of a tree being predicted as **good** stays fairly consistent across the three methods, but the most interesting aspect is the probability of a **poor** rating, which increases across models. This is consistent with the confusion matrixes created for each model.

Given the uneven number of data points available for the varying health conditions, I down-sampled each health rating to the smallest number of points in a given category (Point = 15, Radius = 15, LiDAR = 13). When the predictive models were ran with equal category sizes, the results were statistically significant for all three pixel selection models. The point and radius method models correctly predicted the health ratings for most of the **poor** and **good** rated trees but not for **fair** rated trees, which is the opposite of what we saw with the previous models. The LiDAR model

had the highest proportion of correctly predicted health ratings across all three health categories (Figure 3.13).

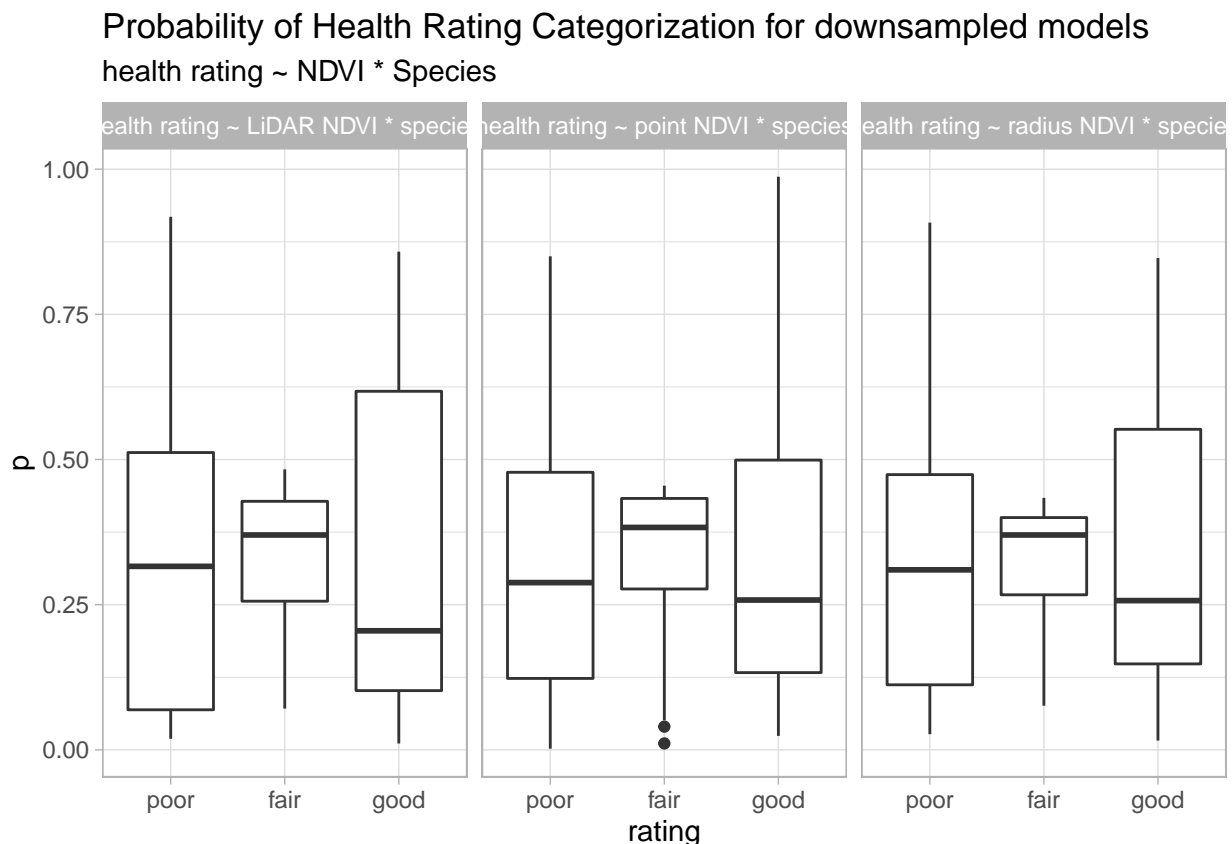


Figure 3.12: Probability of Assignment Analysis with Downsampled Data

I repeated the probability of assignment analysis with the downsampled models (figure 3.12). The probabilities of assignment to each health category are much more even now, though the average probability for a **fair** prediction is still higher than the average probability of a **poor** or **good** rating prediction.

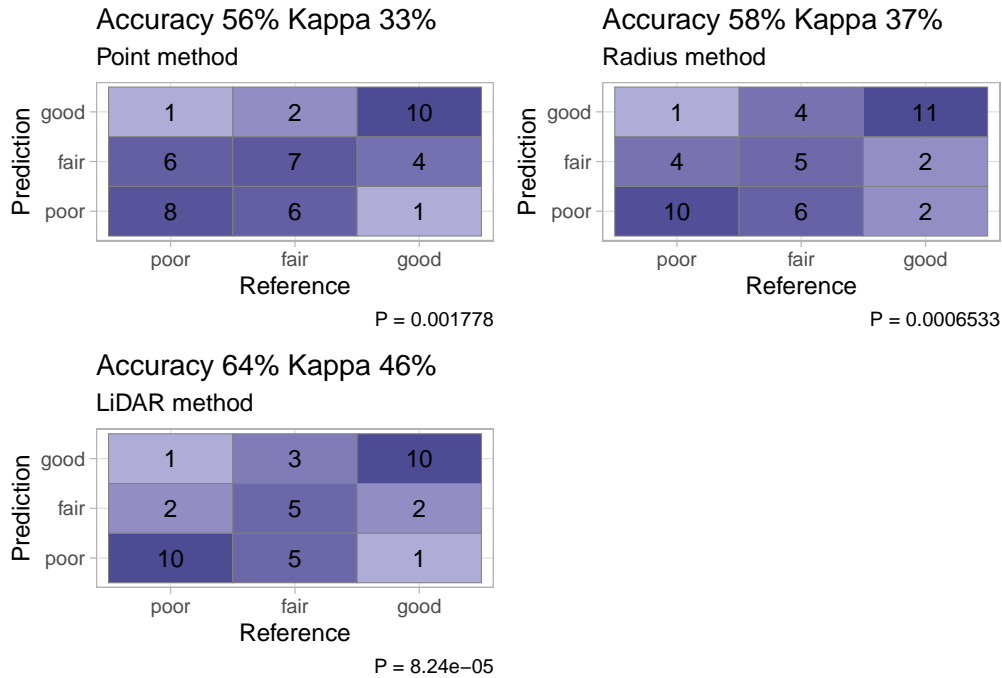


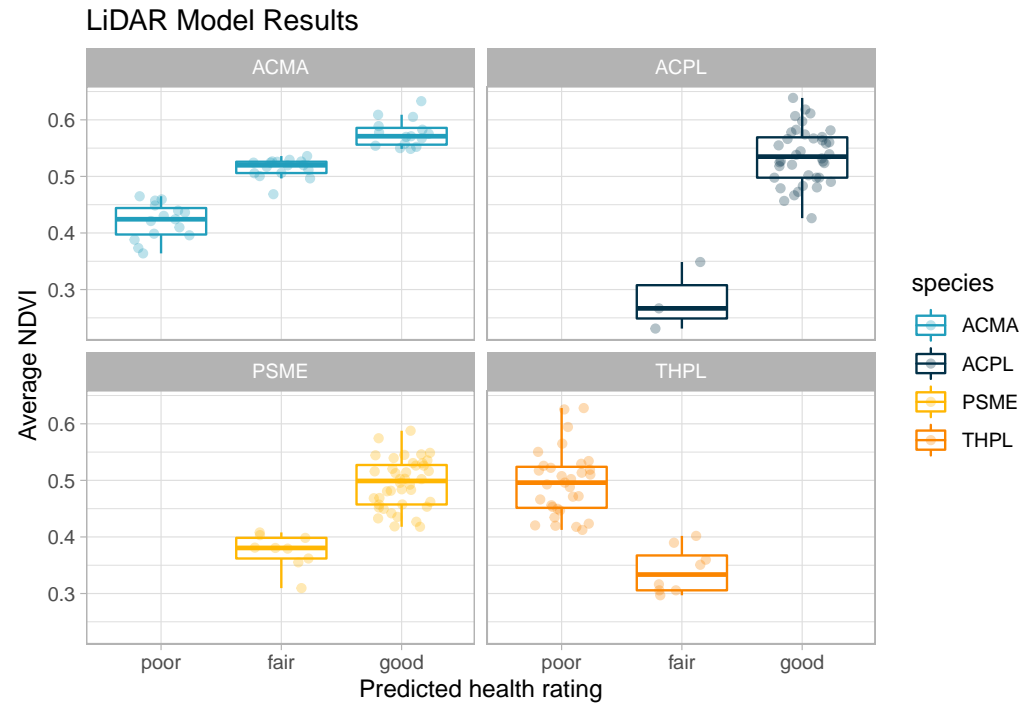
Figure 3.13: Confusion matrixes for downsampled predictive models

Table 3.8: Counts of each species in stratified random sample of park and street trees after LiDAR processing and NDVI calculation.

| Species | Count |
|---------|-------|
| ACMA | 46 |
| ACPL | 41 |
| PSME | 49 |
| THPL | 39 |

To ensure that the results of the downsampled LiDAR data model were not caused by the random downsampling, I ran the model 6 times with different random samples each time (Appendix ??). While the values of each predicted category did differ, the p-value for the model was significant for each test. The accuracy values ranged from 54% to 67%, and the kappa values ranged from 31% to 50% (Table A.3). I used the final downsampled LiDAR model to predict health rating for a random sample of 100 park and 100 street trees, with LiDAR calculated NDVI values. Due to the data loss in the LiDAR processing, the final data set contains 175 trees (85 street trees, 90 park trees) (Table 3.8). This data was input into the final LiDAR model, created with the downsampled data. A health rating was predicted based on NDVI

and tree species. The resulting health predictions were graphed along with sample NDVI (Figure @ref(fig: final-lidar-plot)). For ACMA, there is a clear relationship between sample NDVI and health prediction which matches that seen in earlier data analysis. For ACPL, there is a large difference between the NDVI of **fair** and **good** trees, which also appears for PSME. for the THPL predictions, the average NDVI for **poor** trees is higher than those for **fair** trees.



Chapter 4

Discussion

INTRO PARAGRAPH SUMMARIZING RESULTS

4.1 Strengths and limitations of different delineation techniques

The three pixel selection methods (point, radius, and LiDAR) were used to help answer the question “which pixels are we using?”

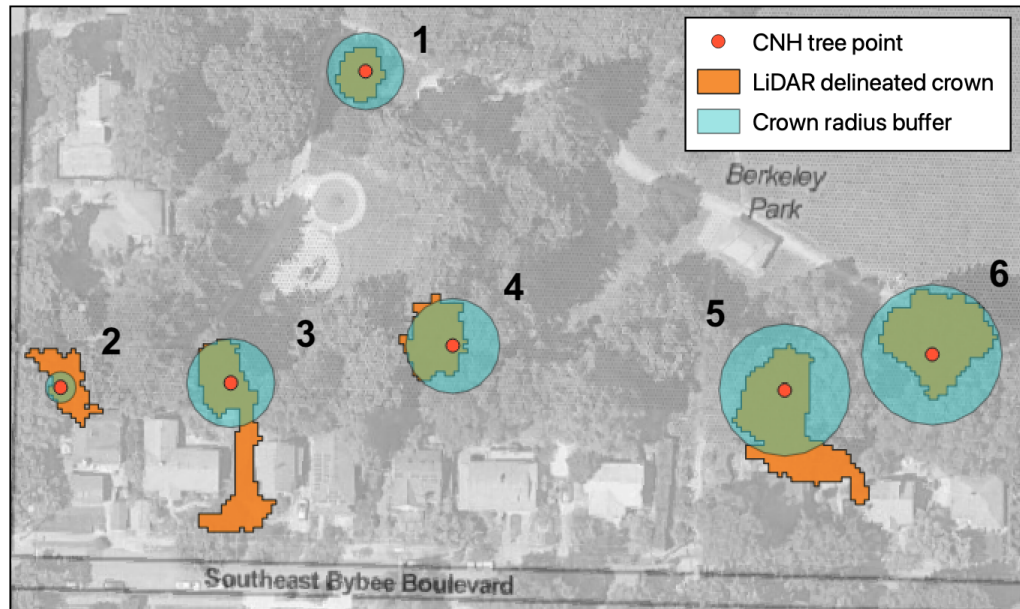


Figure 4.1: Point, Radius, and LiDAR pixel selection methods for Berkeley Park with numbered trees

The point method is the simplest method, obtaining a single NDVI value from

the individual pixel that spatially contains an individual tree location point. The statistically significant difference in the NDVI values for trees categorized as **fair** and **good** seems to be primarily driven by the THPL data.

Given that only one pixel value is used to represent the NDVI of an entire tree in the point method, that single pixel likely misrepresents the health of the tree. If the location point is incorrect, the NDVI value may not belong to the tree of interest. The pixel method NDVI values statistically significantly higher than the NDVI values obtained through the other two pixel selection methods. This can be attributed to the use of a single pixel rather than an average of pixel NDVI values. The approximated center of the tree represented by the tree location point will generally be greener than pixels on the edge because the NDVI value for a pixel is the average NDVI for all data within that pixel, and the central pixel likely contains mostly tree canopy, and ideally little to no information on ground cover surrounding the tree. This is emphasized in figure 4.1, which highlights the large variance in pixel selection extent for the three methods and how much data is missed by the point method.

The radius method averages the NDVI values of pixels within a buffered circle with the size defined by the measured or predicted tree canopy width. This data had a statistically significant difference in average NDVI values between **good** and **poor** categorized trees as well as **good** and **fair** categorized trees. There is a larger difference between **fair** and **good** than **fair** and **poor**, which is also seen in the point method data.

Where the scope of the pixel data is too narrow (only using the value of a singular pixel) the scope of the radius method can be too broad and pixels belonging to other trees will be included.

A large issue that can arise with the radius method data is the overlapping of tree crowns, and pixels being used in the NDVI analysis for multiple trees (Figure ???. Overlapping crowns is an issue that often arises with tree crown delineation. To deal with this, Xiao et al. (2005) chose to exclude any trees with overlapping crowns from the final analysis. Fang et al. (2020) used a version of the radius method where they calculated an average canopy width and used that standardized size (a radius of 4.55 m) to extract their NDVI averages for each tree. The paper does not mention how they dealt with overlapping tree crowns, but perhaps their trees were widely distributed enough and the radius of interest was small enough that their values did not experience overlap. Using LiDAR as a pixel selection method has the benefit of additional pixel data like the radius method, but no overlapping crowns.

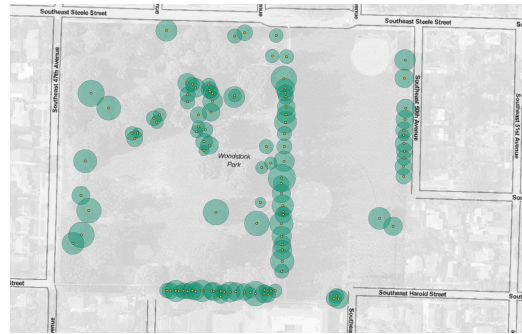


Figure 4.2: Examples of tree crown buffers from radius method data with overlapping crowns for park trees (left) and street trees (right). While the frequency of overlapping crowns is much higher for the park example, it is still apparent in the street trees as well. Given that these figures only include trees of the canary species, the occurrence of overlapping tree canopies is likely even higher than this.



Figure 4.3: Examples of tree crown buffers from radius method data with overlapping crowns for park trees (left) and street trees (right). While the frequency of overlapping crowns is much higher for the park example, it is still apparent in the street trees as well. Given that these figures only include trees of the canary species, the occurrence of overlapping tree canopies is likely even higher than this.

The LiDAR tree crown delineation was by far the most intensive pixel selection method tested in this thesis, but was the most effective for modeling purposes. In some cases (such as trees 1, 4, and 6 in figure 4.1) the LiDAR delineation appears to be highly effective in creating a polygon that is representative of a tree's crown, without the inclusion of overlapping areas. However, there are cases (such as trees 2, 3, and 5) where the canopy delineation algorithm creates canopies for trees that are larger than reality. The LiDAR pixel selection method also led to the most statistically significant predictive models. Using LiDAR for canopy delineation is complicated, but it is also quite effective.

Given the overall results of the three methods, I believe that the radius and LiDAR methods are both valid choices for tree crown delineation and pixel selection, but can have different intended uses that will maximize the benefits of each model. The radius method is fairly easy when compared to the LiDAR processing. Especially if the data already contains a crown width measurement, the radius method can be a decently simple method of selecting pixels for NDVI assessment. However, if the goal is maximizing the accuracy of the tree crown delineations, the the LiDAR method is the best approach.

4.2 Evaluation of Tree Health Predictions

The final LiDAR model for predicting tree health based on NDVI and species had promising results for the two maple species, especially ACMA. The ACMA health predictions mirrored the pattern seen in the measured health condition and LiDAR calculated NDVI. With ACPL, the predictions showed effective separation of **fair** and **good**, but no predictions of **poor** trees. A limitation for all of the models is sample size. The models were only statistically significant when the health rating groups were downsampled to equal sizes, and the level of statistical significance and predictions varied depending on the sample of trees that was included in the downsampled data. Additionally, the distribution of species across health rating with the downsampled data is uneven (table 4.1. Due to data loss during the LiDAR canopy delineation, the final dataset used for model training had no PSME individuals rated as **poor** health. In the predictions, no PSME individuals were rated as **poor**, which in context of the training dataset makes complete sense. If there is no basis for a prediction of a specific health rating, that health rating will not be predicted. For all species, an overall larger sample size would likely improve the predictions and the model as a whole. This is easier said than done, since while collecting field data and health analyses, the species sampled can be controlled by selection, but their health cannot be. In order to create a predictive model that works for more than just ACMA, it is necessary to increase the size of data for model training.

Table 4.1: Count of Species and Ratings in final dataset used for LiDAR downsampled model training

| Species | Count Poor | Count Fair | Count Good |
|---------|------------|------------|------------|
| ACMA | 6 | 3 | 2 |
| ACPL | 2 | 2 | 9 |
| THPL | 5 | 5 | 1 |
| PSME | 0 | 3 | 1 |

4.3 Impact of Functional Tree Type and Species on Tree Health Assessments

In all models and data analysis, very different patterns were seen between the broadleaf deciduous trees (ACMA and ACPL) and the coniferous evergreen trees (PSME and THPL). This is at least partially due to the functional tree type and how these trees respond to environmental conditions and declining health. Deciduous trees lose their leaves every fall, and grow new ones every spring. Since their vegetation has a shorter lifespan of one growing season, it is much more sensitive to sudden and extreme environmental impacts. Declining health can be seen in broadleaf trees as leaf damage or scorching, discoloration in the foliage, or a decrease in the number of leaves grown each year (CITE). Conversely, coniferous evergreen trees retain their foliage after each growing season, adding new growth on to the end of branches. Since evergreen trees cannot regrow all their foliage after a year with harsh environmental conditions, their response is often seen in the loss of branches and a reduction in overall canopy cover (CITE). Because of these variations in response types, the models including functional type as a predictor variable had higher levels of accuracy than the method only using NDVI.

For each of the three pixel selection method models, the model that differentiated the predictions by species was the most accurate. Because of the differences in functional type and other species-specific characteristics, it makes sense that increasing the specificity of the model to species would improve the predictions. This additional separation of tree species also highlighted the utility of the final predictive model for separating ACMA individuals into distinct health categories based on NDVI, but this did not hold true for the ACPL predictions.

Separating the predictions by species was consistently more effective than separating by functional type. Like with the tree crown delineations, the species differentiation was the most effective, but functional type specificity can do in a pinch. For

the purpose of obtaining a rough understanding of NDVI across various functional types of trees, then specifying functional type instead of species will paint an adequate picture of tree health. However, to maximize accuracy of health predictions, species separation

4.4 Limitations of Satellite Imaging

While the use of satellite imaging for urban ecology applications is becoming more frequent, there are still numerous avenues that need additional research and improvement. The first of those is documentation and access.

Another limitation of satellite imaging for tree health assessment is seasonality. Especially with deciduous trees, NDVI obtained outside of the peak growing season will not be able to get anywhere close to an accurate health rating based on greenness. By filtering for satellite images collected during the peak on-leaf period, this variability can be limited. Fang et al. (2020) compared satellite images from June, July, and August and found that the July image, which was obtained for the peak on-leaf period for Washington D.C., was the most accurate and effective when examining tree health.

Tree species also has a large impact on NDVI values due to the natural variability in tree vegetation color. Coniferous trees are generally much darker in color than deciduous trees. Between deciduous tree species, there can be extensive variation in color as well. Some trees have vegetation that naturally appears reddish or purple, so these species would require a different type of vegetation index for health modeling than species that are naturally quite green.

4.5 Open Source Data and Accessible Science

When beginning this thesis, a large goal of mine was to use only open source and freely accessible data sources and programs. For the most part, I was able to meet this goal. The satellite data I used was accessed through PlanetScope's Education and Research Program, which provided me with limited, non-commercial access to PlanetScope satellite imagery. This is accessible after a short application, provided that the applicant has a college or university email address. Both the street and park tree inventories were publicly available through Portland's GIS opendata site, and the LiDAR canopy height model was available through Portland's Regional Land Information System (RLIS). The one processing task I was not able to do on an open

source software was the file conversion of the LiDAR CHM. It is only available for download as a File Geodatabase, which is a proprietary ArcGIS file type. In order to be able to utilize it in QGIS, which is an open source GIS software, I had to open the CHM file in ArcGIS through Reed's institutional access, and export it as a .tif file type. This is unfortunate, because it is very possible for Portland's RLIS site to host the canopy height model in a different format. While many of the data sources I used were openly accessible, throughout this process it became apparent that the processing techniques were not. I had to use three different platforms (RStudio, QGIS, and Python) to conduct the work for this thesis.

Satellite imagery with a 3m pixel size is relatively high resolution, but less so in the context of urban ecology. The satellite data used in Fang et al. (2020) was eight multispectral bands with a resolution of 1.2m, and one panchromatic band with a spatial resolution of 0.3m. Satellite imagery with this resolution or higher is unavailable to the public or even for research purposes without payment or subscription to a data hosting site. When I was working with PlanetScope data in the summer of 2020, I reached out to Planet Labs about gaining access to their higher resolution data products and the possibility of purchasing individual access to the data if needed. I was told that Planet does minimum purchase orders of \$10,000 USD. While the availability of the basic satellite imagery through Planet Labs is an incredible resource, it is frustrating that the high price tag severely limits the accessibility of much of their data.

4.6 Future Directions

For future work in modeling tree health, a combined pixel selection using both the Radius and LiDAR methods could have promising results. By calculating the areas of both the radius buffer circles and the LiDAR canopies for each tree and using the smaller of the two areas, the amount of overlapping tree crowns will be minimized along with the overestimated LiDAR delineated crowns. Other studies have used an NDVI threshold to exclude non-vegetation pixels, which was unrealistic to do given the pixel size of the data I used. However, if this work could be repeated with higher resolution NDVI data, masking of pixels based on an NDVI threshold may be effective.

Additionally, altering the model to predict two conditions (**healthy** vs **unhealthy**) may be more accurate, since all three pixel selection methods had statistically significant differences between the **good** and **fair** categories. Splitting the trees into two health categories instead of three would increase the number of

unhealthy trees predicted, since the trees categorized as **fair** would be split between the **healthy** and **unhealthy** ratings.

Given the ineffective nature of my model for predicting the health categorizations for coniferous trees, a different direction may be needed. One possible method of remote health analysis for coniferous trees could be canopy cover.

4.7 Conclusion

Appendix A

Supplementary Data

CNH Project Neighborhoods and Classification

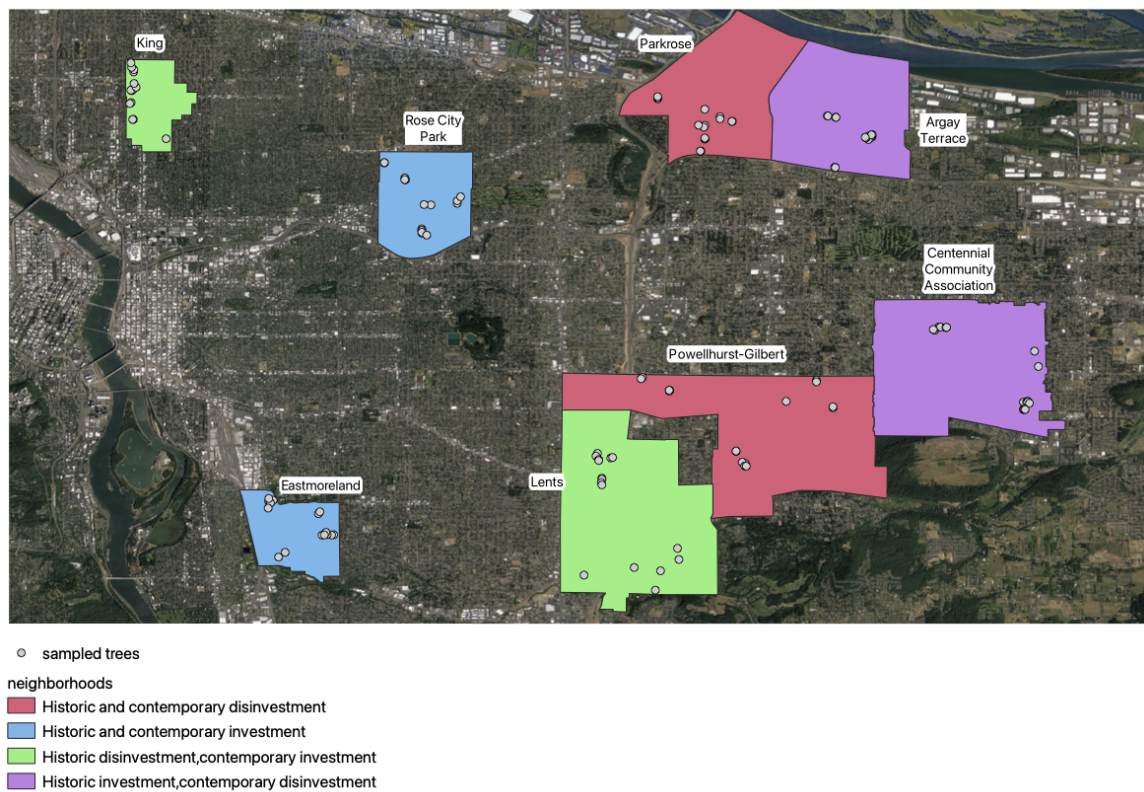


Figure A.1: CNH sampled neighborhoods with classification

Variable types for tree inventories

Table A.1

| Variable name | Street trees | Park trees | CNH2 trees |
|---|--------------|------------|------------|
| % canopy missing or dead | - | - | x |
| Address | x | - | - |
| Canopy base height | - | - | x |
| Carbon sequestration (lb) | - | x | - |
| Carbon sequestration (value) | - | x | - |
| Carbon storage (lb) | - | x | - |
| Carbon storage (value) | - | x | - |
| Chlorophyll fluorescence | - | - | x |
| Common name | x | x | x |
| Crown width | - | x | x |
| DBH | x | x | x |
| Edible (Y/N) | x | x | - |
| Evidence of injury, infestation, or disease | - | - | x |
| Evidence of watering | - | - | x |
| Family | x | x | x |
| Foliage chlorophyll content | - | - | x |
| Foliage scorching | - | - | x |
| Functional type | x | x | - |
| Genus | x | x | x |
| Ground cover type | - | - | x |
| Health Condition | x | x | x |
| Inventory Date | x | x | x |
| Leaf area index | - | - | x |
| Light level | - | - | x |
| Location (lat/long) | x | x | x |
| Mature size (S/M/L) | x | x | - |
| Native (Y/N) | - | x | - |
| Nearest neighbor | - | - | x |
| Neighborhood | x | - | x |
| Nuisance (Y/N) | - | x | - |
| Origin | - | x | - |

| | | | |
|---|---|---|---|
| Park name | - | x | x |
| Pollution removal (oz) | - | x | - |
| Pollution removal (value) | - | x | - |
| Presence of buildings within 25m | - | - | x |
| Scientific name | x | x | x |
| Site development | x | - | - |
| Site size | x | - | - |
| Site type | x | - | x |
| Site width | x | - | - |
| Species | x | x | x |
| Species factoid | - | x | - |
| Stomatal conductance | - | - | x |
| Stormwater (ft) | - | x | - |
| Stormwater (value) | - | x | - |
| Structural value | - | x | - |
| Temperature (canopy, bole, air, ground) | - | - | x |
| Total annual services | - | x | - |
| Tree height | - | x | x |
| Volunteer or Staff? | x | x | - |
| Wind speed | - | - | x |
| Wires (Y/N) | x | - | - |

Scene products and satellite swaths

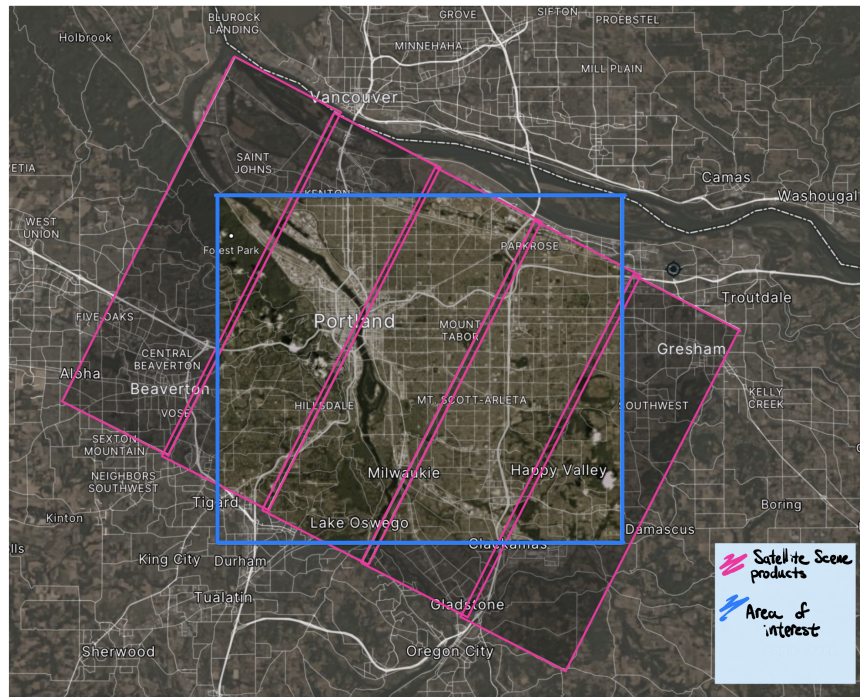


Figure A.2: Satellite scene product swaths for 2016 PlanetScope data

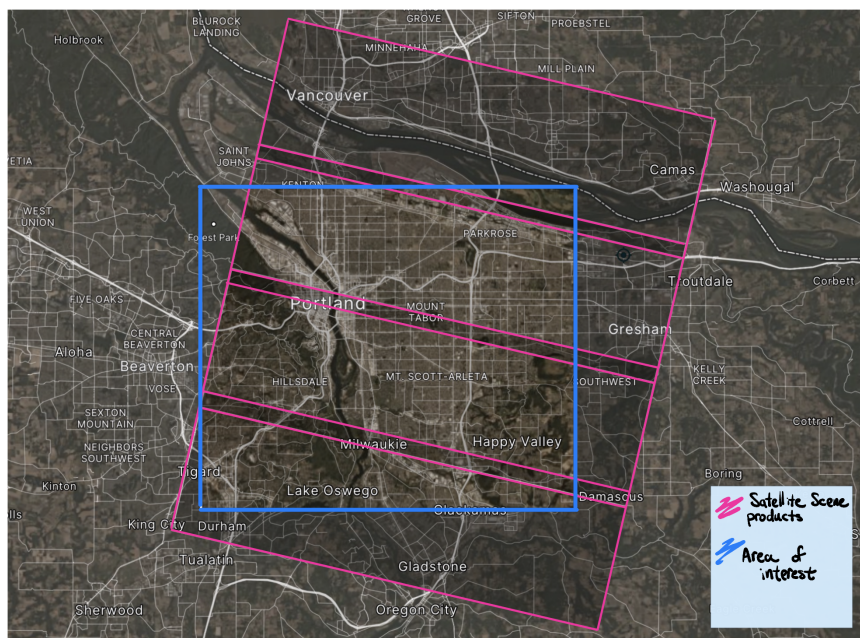


Figure A.3: Satellite scene product swaths for 2019 PlanetScope data

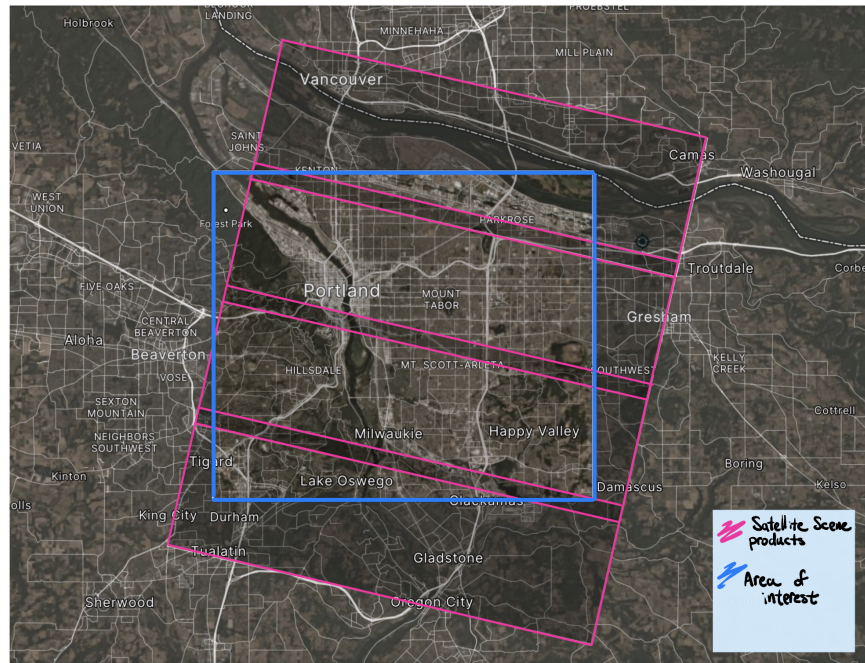


Figure A.4: Satellite scene product swaths for 2021 PlanetScope data

Model Tests

Model testing for Tree Height predictions

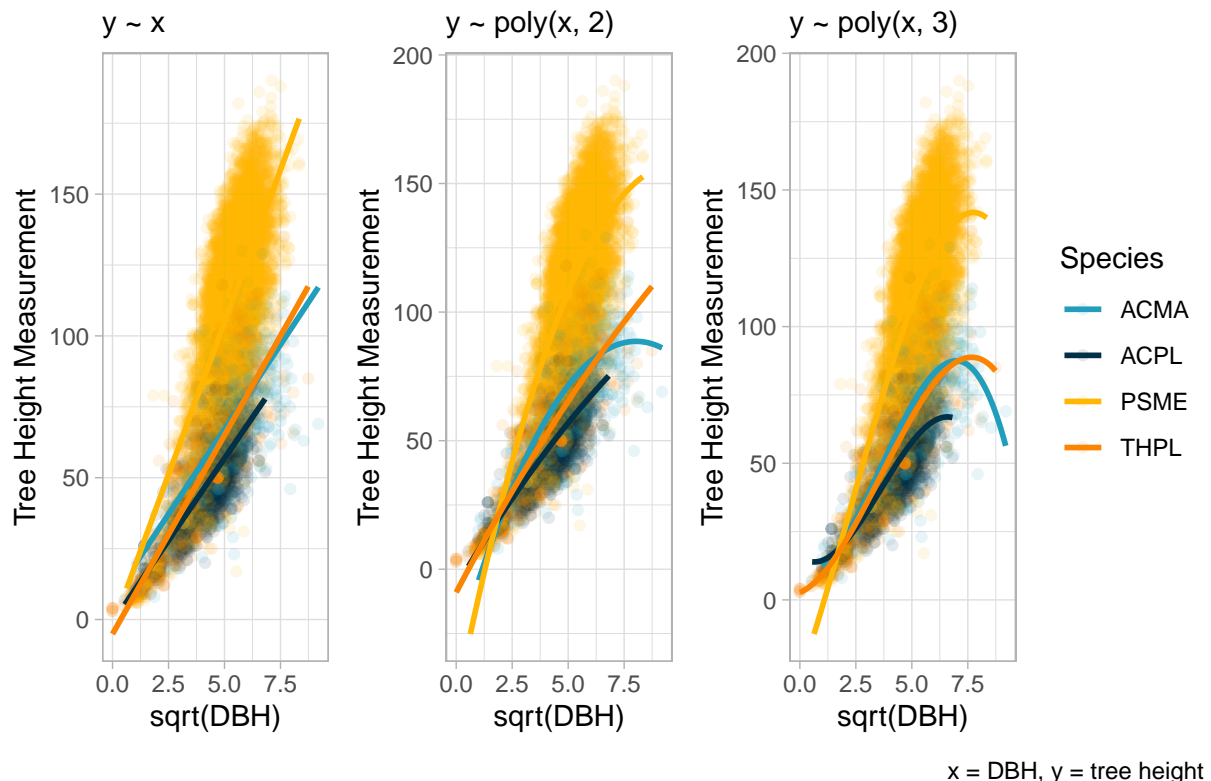


Figure A.5: Predicting tree height from tree species and DBH. A linear, second degree, and third degree polynomial were tested, and raw polynomials were used.

Model testing for Canopy Width predictions

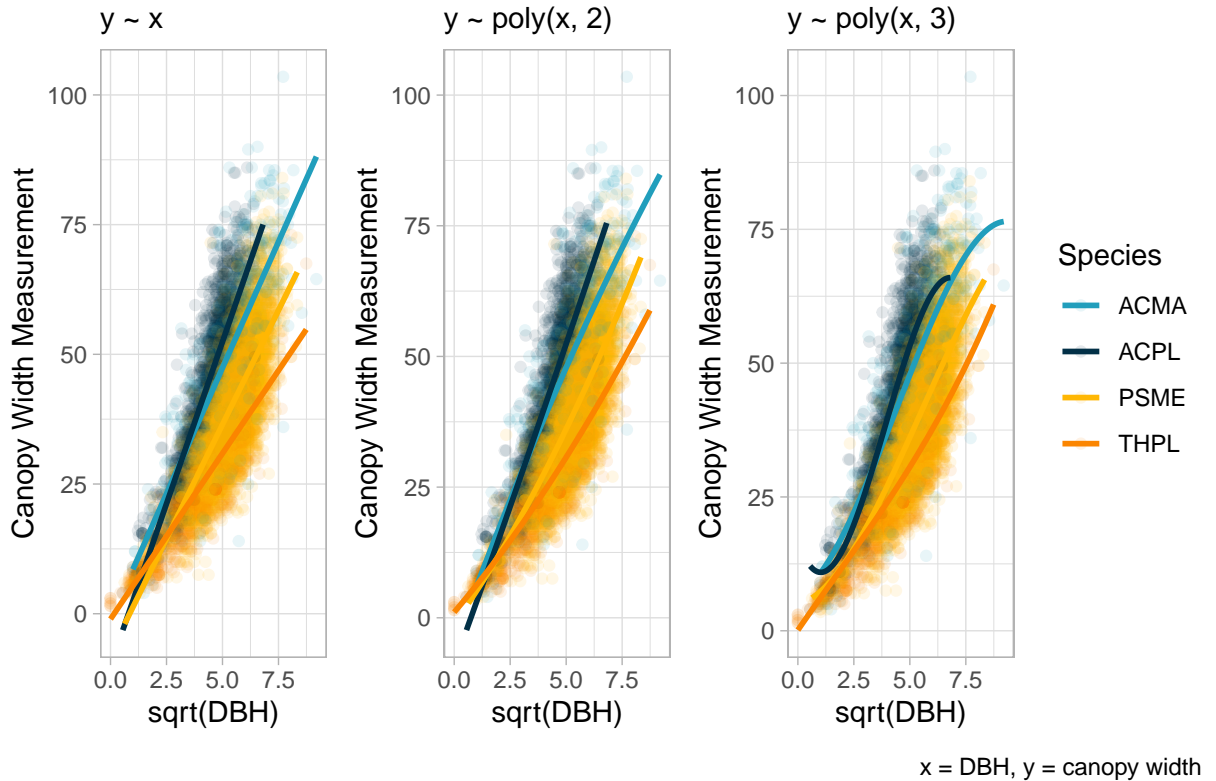


Figure A.6: Predicting canopy width from tree species and DBH. A linear, second degree, and third degree polynomial were tested, and raw polynomials were used.

Height model results and predictions

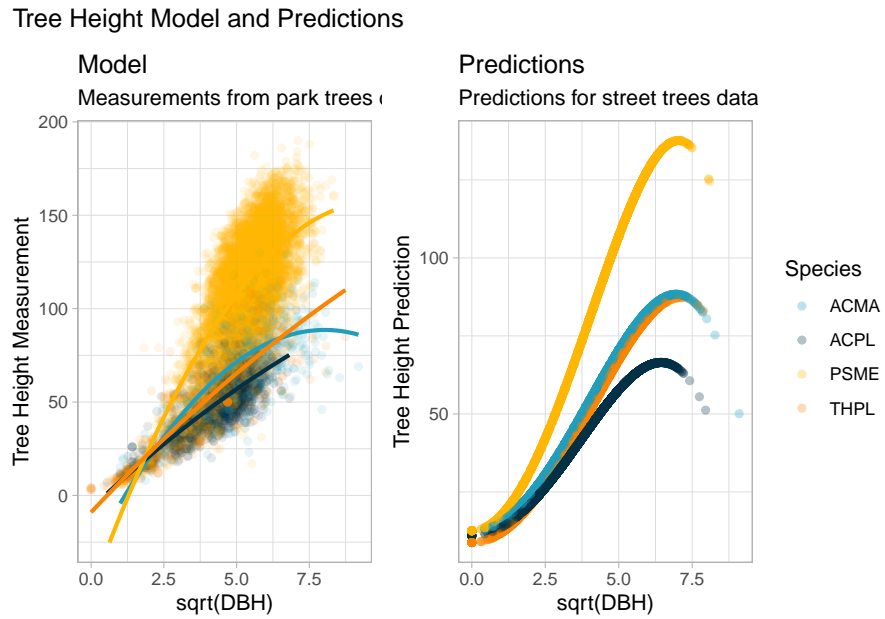


Figure A.7: Predictive model for tree height from measured DBH. A second order polynomial regression was used in order to account for the variation between species. (Adjusted R-squared = 0.7834, P < 2.2e-16)

Tree Height and Crown Width Predictive Model Equations

ACMA equations: ($x = \text{DBH}$)

$$\text{Tree Height} = 12.308 + 3.139x - 0.032x^2 \quad (\text{A.1})$$

$$\text{Crown Width} = 12.117 + 1.721x - 0.0122x^2 \quad (\text{A.2})$$

ACPL equations: ($x = \text{DBH}$)

$$\text{Tree Height} = -1.359 - 0.464x + 0.000203x^2 \quad (\text{A.3})$$

$$\text{Crown Width} = -7.155 + 0.894x - 0.0153x^2 \quad (\text{A.4})$$

PSME equations: ($x = \text{DBH}$)

$$\text{Tree Height} = 0.2448 + 1.916x - 0.0187x^2 \quad (\text{A.5})$$

$$\text{Crown Width} = -4.640583 - 0.3867x + 0.0046x^2 \quad (\text{A.6})$$

THPL equations: ($x = \text{DBH}$)

$$\text{Tree Height} = -3.5146 - 0.0388x + 0.00178x^2 \quad (\text{A.7})$$

$$\text{Crown Width} = -4.953 - 0.5939x + 0.00512x^2 \quad (\text{A.8})$$

Additional Information on Health Predictive Model

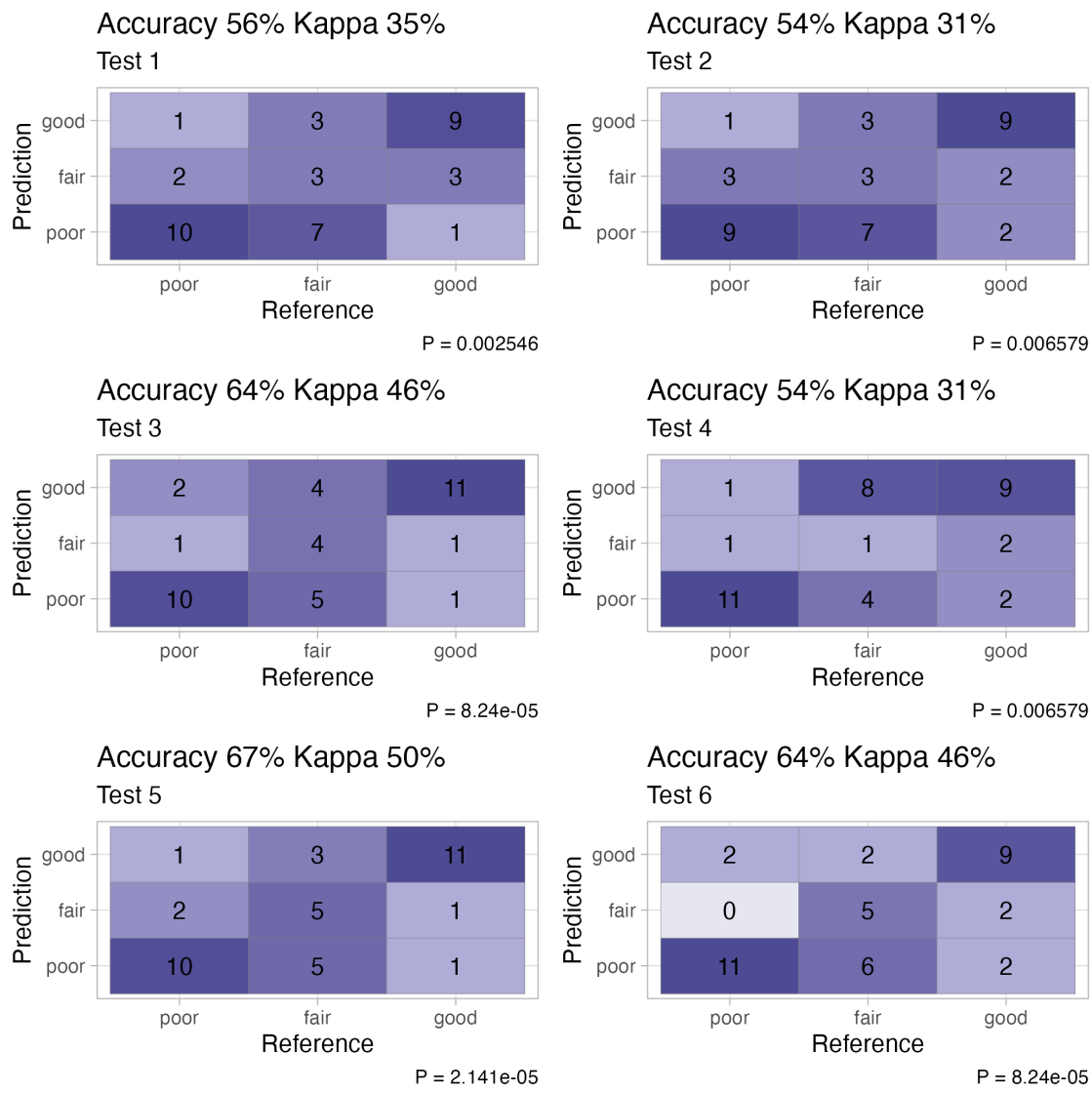
Table A.2: For each predictive model for tree health, this table contains the pixel selection method and predictors used, as well as the resulting accuracy, kappa, and p-value calculated in the confusion matrixes.

| NDVI pixel method | Predictors | Accuracy | Kappa | P-value |
|-------------------|------------------|----------|-------|---------|
| Point method | NDVI | 61% | 0% | 0.54120 |
| Radius method | NDVI | 61% | 3% | 0.54120 |
| LiDAR method | NDVI | 63% | 10% | 0.38400 |
| Point method | NDVI * tree type | 63% | 15% | 0.31630 |
| Radius method | NDVI * tree type | 63% | 16% | 0.31630 |
| LiDAR method | NDVI * tree type | 67% | 23% | 0.13340 |
| Point method | NDVI * species | 64% | 23% | 0.25040 |
| Radius method | NDVI * species | 64% | 24% | 0.25040 |
| LiDAR method | NDVI * species | 68% | 33% | 0.09396 |

Table A.3: Statistical values for LiDAR predictive model tests

| Test | Accuracy | Kappa | P-Value |
|--------|----------|-------|-----------|
| test 1 | 56% | 35% | 0.0025460 |
| test 2 | 54% | 31% | 0.0065790 |
| test 3 | 64% | 46% | 0.0000824 |
| test 4 | 54% | 31% | 0.0065790 |
| test 5 | 67% | 50% | 0.0000214 |
| test 6 | 64% | 46% | 0.0000824 |

LiDAR model tests



Predicted Health Rating and Species Counts

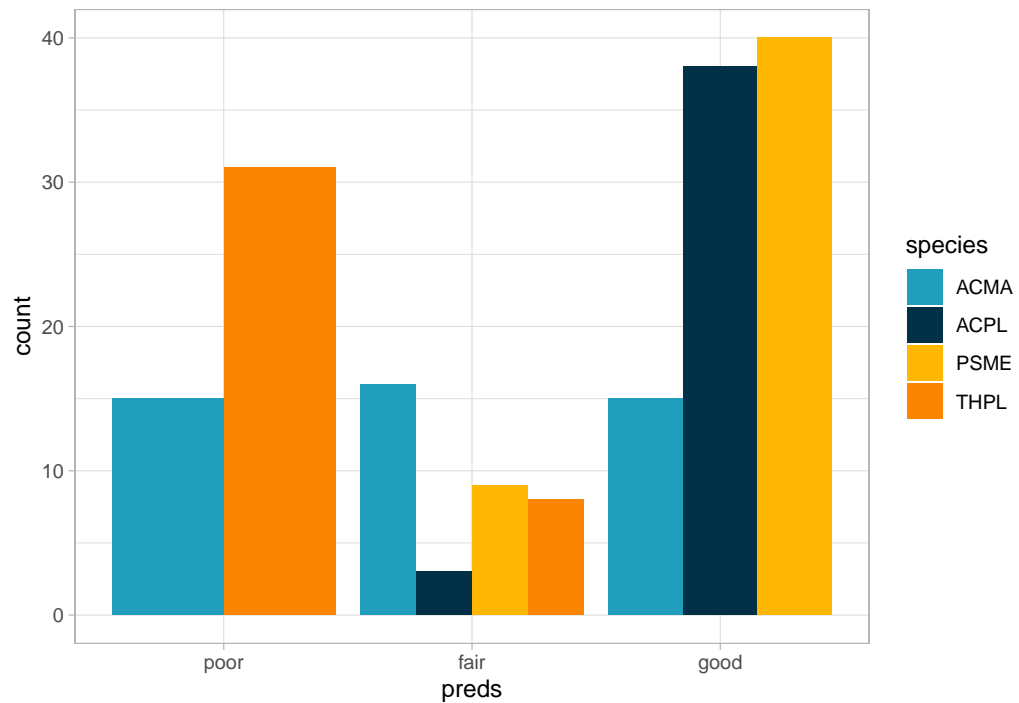


Figure A.8: Graph of species counts for LiDAR health predictions

Appendix B

Code

This second appendix includes all of the R chunks of code that were hidden throughout the document to help with readability and/or setup.

In Chapter 2:

Portland Tree Inventory counts and calculations

```
street_counts <- get_pdxTrees_streets() %>%
  filter(Species %in% c("ACMA", "ACPL", "PSME", "THPL")) %>%
  mutate(year = year(Inventory_Date)) %>%
  dplyr::select(Species, year) %>%
  add_count(Species, year) %>%
  distinct() %>%
  group_by(Species) %>%
  mutate(Total = sum(n)) %>%
  rename(Count_2016 = n) %>%
  filter(year == 2016) %>%
  dplyr::select(-year)

park_counts <- get_pdxTrees_parks() %>%
  filter(Species %in% c("ACMA", "ACPL", "PSME", "THPL")) %>%
  mutate(year = year(Inventory_Date)) %>%
  dplyr::select(Species, year) %>%
  add_count(Species, year) %>%
  distinct() %>%
  group_by(Species) %>%
  mutate(Total = sum(n)) %>%
  rename(Count_2019 = n) %>%
```

```
filter(year == 2019) %>%
dplyr::select(-year)
```

Calculating NDVI from satellite imagery

```
import rasterio
import numpy

files = ["1", "2", "3", "4"] # unique file identifiers
folder = "ndvi_calc_thesis/files" # folder with the raw files
date = "20210726" # product date

for i in range(len(files)):
    filenum = files[i]
    image_file = folder+"/"+date+"_"+filenum+"_AnalyticMS.tif"

    metafile = folder+"/"+date+"_"+filenum+"_AnalyticMS_metadata.xml"
    print(image_file)
    print(metafile)

    # Load red and NIR bands -
    # note all PlanetScope 4-band images have band order BGRN

    with rasterio.open(image_file) as src:
        band_red = src.read(3)

    with rasterio.open(image_file) as src:
        band_nir = src.read(4)

    from xml.dom import minidom

    xmldoc = minidom.parse(metafile)
    nodes = xmldoc.getElementsByTagName("ps:bandSpecificMetadata")

    # XML parser refers to bands by numbers 1-4
    coeffs = {}
    for node in nodes:
        bn = node.getElementsByTagName("ps:bandNumber")[0].firstChild.data
        if bn in ['1', '2', '3', '4']:
            i = int(bn)
            value = node.getElementsByTagName("ps:reflectanceCoefficient")[0].firstChild.data
            coeffs[i] = float(value)

    red = band_red * coeffs[3]
    nir = band_nir * coeffs[2]
```

```

coeffs[i] = float(value)

# Multiply by corresponding coefficients
band_red = band_red * coeffs[3]
band_nir = band_nir * coeffs[4]

# Allow division by zero
numpy.seterr(divide='ignore', invalid='ignore')

# Calculate NDVI
ndvi = (band_nir.astype(float) - band_red.astype(float)) / (band_nir + band_red)

# Set spatial characteristics of the output object to mirror the input
kwargs = src.meta
kwargs.update(
    dtype=rasterio.float32,
    count=1)

# Set name for new NDVI file
newfile = folder + '/ndvi_' + date + "_" + filenum + '.tif'

# Create the file
with rasterio.open(newfile, 'w', **kwargs) as dst:
    dst.write_band(1, ndvi.astype(rasterio.float32))

```

LiDAR canopy delineation

```

library(rgdal)
library(imager)
library(raster)
library(ForestTools)

options(rgdal_show_exportToProj4_warnings = "none")

## Loading raster data
EML_CHM <- raster("~/Desktop/thesis_data/lidar_crown/clipped_lidar.tif")

## Loading tree points
all_ttops <- shapefile("~/Desktop/thesis_data/lidar_crown/all_tree_points_for_delin.tif")

# delineate tree crowns inputs: my tree points, LiDAR data
crownsPoly <- mcws(treetops = all_ttops, CHM = EML_CHM, format = "polygons",

```

```

minHeight = 20, verbose = TRUE)

# export file
writeOGR(crownsPoly,("~/Desktop/thesis_data/lidar_crown", "canopy_delin_polygons_poly",
  driver = "ESRI Shapefile")

```

In Chapter 3:

Model for Tree Height and Canopy Width

```

# create model for heights
heights <- lm(Tree_Height ~ poly(DBH, degree = 2, raw = T) *
  Species, data = my_park)
summary(heights)

# create model for crown width
cr_width <- lm(crown_width ~ poly(DBH, degree = 2, raw = T) *
  Species, data = my_park)
summary(cr_width)

# load street data, filter to relevant species
my_street <- pdxTrees:::get_pdxTrees_streets() %>%
  filter(Species %in% c("ACPL", "THPL", "PSME", "ACMA"))

# run street trees through both models
my_street_2 <- my_street %>%
  mutate(width_preds = predict(cr_width, my_street, se.fit = FALSE),
    height_preds = predict(heights, my_street, se.fit = F))

# export data file write_csv(my_street,
# 'data/my_street_2.csv')

# graphing
p_height_model <- my_park %>%
  ggplot(aes(x = sqrt(DBH), y = Tree_Height, color = Species)) +
  geom_point(alpha = 0.1) + scale_color_manual(values = species_pal) +
  geom_smooth(method = "lm", se = F, formula = y ~ poly(x,
    degree = 2, raw = T)) + labs(subtitle = "Measurements from park trees data",
    y = "Tree Height Measurement", title = "Model") + guides(color = "none")

p_width_model <- my_park %>%
  ggplot(aes(x = sqrt(DBH), y = crown_width, color = Species)) +

```

```

geom_point(alpha = 0.1) + scale_color_manual(values = species_pal) +
  geom_smooth(method = "lm", se = F, formula = y ~ poly(x,
    degree = 2, raw = T)) + labs(subtitle = "Measurements from park trees data",
    y = "Canopy Width Measurement", title = "Model") + guides(color = "none")

s_height_preds <- my_street_2 %>%
  ggplot(aes(x = sqrt(DBH), y = height_preds, color = Species)) +
  geom_point(alpha = 0.3) + scale_color_manual(values = species_pal) +
  labs(subtitle = "Predictions for street trees data", y = "Tree Height Prediction",
    title = "Predictions")

s_width_preds <- my_street_2 %>%
  ggplot(aes(x = sqrt(DBH), y = width_preds, color = Species)) +
  geom_point(alpha = 0.3) + scale_color_manual(values = species_pal) +
  labs(subtitle = "Predictions for street trees data", y = "Canopy Width Prediction",
    title = "Predictions")

```

Point Method Modeling

```

point_all <- polr(health_rat ~ sample_ndvi, Hess = TRUE, data = cnh_point)
brant::brant(point_all)

point_all_preds <- predict(point_all, cnh_point)
cfm_p_all <- confusionMatrix(point_all_preds, cnh_point$health_rat)

p_all <- ggplotConfusionMatrix(cfm_p_all)

point_type <- polr(health_rat ~ sample_ndvi * tree_type, Hess = TRUE,
  data = cnh_point)
brant::brant(point_type)

point_type_preds <- predict(point_type, cnh_point)
cfm_p_type <- confusionMatrix(point_type_preds, cnh_point$health_rat)

p_type <- ggplotConfusionMatrix(cfm_p_type)

point_species <- polr(health_rat ~ sample_ndvi * species, Hess = TRUE,
  data = cnh_point)
brant::brant(point_species)

point_species_preds <- predict(point_species, cnh_point)
cfm_p_species <- confusionMatrix(point_species_preds, cnh_point$health_rat)

```

```
p_species <- ggplotConfusionMatrix(cfm_p_species)
```

Radius Method Modeling

```
radius_all <- polr(health_rat ~ sample_ndvi, Hess = TRUE, data = cnh_radius)
radius_all_preds <- predict(radius_all, cnh_radius)
cfm_r_all <- confusionMatrix(radius_all_preds, cnh_radius$health_rat)
r_all <- ggplotConfusionMatrix(cfm_r_all)

radius_type <- polr(health_rat ~ sample_ndvi * tree_type, Hess = TRUE,
                     data = cnh_radius)
radius_type_preds <- predict(radius_type, cnh_radius)
cfm_r_type <- confusionMatrix(radius_type_preds, cnh_radius$health_rat)

r_type <- ggplotConfusionMatrix(cfm_r_type)

radius_species <- polr(health_rat ~ sample_ndvi * species, Hess = TRUE,
                       data = cnh_radius)
radius_species_preds <- predict(radius_species, cnh_radius)
cfm_r_species <- confusionMatrix(radius_species_preds, cnh_radius$health_rat)

r_species <- ggplotConfusionMatrix(cfm_r_species)
```

LiDAR Method Modeling

```
lidar_all <- polr(health_rat ~ sample_ndvi, Hess = TRUE, data = cnh_lidar)
lidar_all_preds <- predict(lidar_all, cnh_lidar)
cfm_l_all <- confusionMatrix(lidar_all_preds, cnh_lidar$health_rat)

l_all <- ggplotConfusionMatrix(cfm_l_all)

lidar_type <- polr(health_rat ~ sample_ndvi * tree_type, Hess = TRUE,
                     data = cnh_lidar)
lidar_type_preds <- predict(lidar_type, cnh_lidar)
cfm_l_type <- confusionMatrix(lidar_type_preds, cnh_lidar$health_rat)

l_type <- ggplotConfusionMatrix(cfm_l_type)

lidar_species <- polr(health_rat ~ sample_ndvi * species, Hess = TRUE,
                      data = cnh_lidar)
```

```

lidar_species_preds <- predict(lidar_species, cnh_lidar)
cfm_l_species <- confusionMatrix(lidar_species_preds, cnh_lidar$health_rat)

l_species <- ggplotConfusionMatrix(cfm_l_species)

```

Radius and LiDAR Replications

```

set.seed(2)
test_data_point <- cnh_long %>%
  filter(method == "point") %>%
  group_by(health_rat) %>%
  sample_n(15)

test_point <- polr(health_rat ~ sample_ndvi * species, Hess = TRUE,
  data = test_data_point)
preds_point <- predict(test_point, test_data_point)
cfm_point <- confusionMatrix(preds_point, test_data_point$health_rat)

probs_point_small <- as_tibble(round(predict(test_point, test_data_point,
  type = "p"), 3)) %>%
  pivot_longer(cols = c("good", "fair", "poor"), names_to = "rating",
  values_to = "p") %>%
  mutate(rating = fct_relevel(rating, levels = c("poor", "fair",
  "good")))

gg_point <- ggplotConfusionMatrix(cfm_point) + labs(subtitle = "Point method")

set.seed(7)
test_data_radius <- cnh_long %>%
  filter(method == "radius") %>%
  group_by(health_rat) %>%
  sample_n(15)

test_radius <- polr(health_rat ~ sample_ndvi * species, Hess = TRUE,
  data = test_data_radius)

probs_radius_small <- as_tibble(round(predict(test_radius, test_data_radius,
  type = "p"), 3)) %>%
  pivot_longer(cols = c("good", "fair", "poor"), names_to = "rating",
  values_to = "p") %>%
  mutate(rating = fct_relevel(rating, levels = c("poor", "fair",
  "good")))

```

```
"good")))

preds_radius <- predict(test_radius, test_data_radius)
cfm_radius <- confusionMatrix(preds_radius, test_data_radius$health_rat)

gg_radius <- ggplotConfusionMatrix(cfm_radius) + labs(subtitle = "Radius method")

set.seed(9)
test_data_lidar <- cnh_long %>%
  filter(method == "lidar") %>%
  group_by(health_rat) %>%
  sample_n(13)

test_lidar <- polr(health_rat ~ sample_ndvi * species, Hess = TRUE,
  data = test_data_lidar)

probs_lidar_small <- as_tibble(round(predict(test_lidar, test_data_lidar,
  type = "p"), 3)) %>%
  pivot_longer(cols = c("good", "fair", "poor"), names_to = "rating",
  values_to = "p") %>%
  mutate(rating = fct_relevel(rating, levels = c("poor", "fair",
  "good")))

preds_lidar <- predict(test_lidar, test_data_lidar)
cfm_lidar <- confusionMatrix(preds_lidar, test_data_lidar$health_rat)

gg_lidar <- ggplotConfusionMatrix(cfm_lidar) + labs(subtitle = "LiDAR method")
```

References

- Anderson, L. M., and H. K. Cordell. 1988. "Influence of Trees on Residential Property Values in Athens, Georgia (U.S.A.): A Survey Based on Actual Sales Prices." *Landscape and Urban Planning*, Special Issue: Urban Forest Ecology, 15 (1): 153–64. [https://doi.org/10.1016/0169-2046\(88\)90023-0](https://doi.org/10.1016/0169-2046(88)90023-0).
- Beckmann-Wübbelt, Angela, Annika Fricke, Zita Sebesvari, Iulia Almeida Yakouchenkova, Katrin Fröhlich, and Somidh Saha. 2021. "High Public Appreciation for the Cultural Ecosystem Services of Urban and Peri-Urban Forests During the COVID-19 Pandemic." *Sustainable Cities and Society* 74 (November): 103240. <https://doi.org/10.1016/j.scs.2021.103240>.
- Brant, Rollin. 1990. "Assessing Proportionality in the Proportional Odds Model for Ordinal Logistic Regression." *Biometrics* 46 (4): 1171–78. <https://doi.org/10.2307/2532457>.
- Breshears, David D., Neil S. Cobb, Paul M. Rich, Kevin P. Price, Craig D. Allen, Randy G. Balice, William H. Romme, et al. 2005. "Regional Vegetation Die-Off in Response to Global-Change-Type Drought." *Proceedings of the National Academy of Sciences* 102 (42): 15144–48. <https://doi.org/10.1073/pnas.0505734102>.
- Byer, Sarah, and Yufang Jin. 2017. "Detecting Drought-Induced Tree Mortality in Sierra Nevada Forests with Time Series of Satellite Data." *Remote Sensing* 9 (9): 929. <https://doi.org/10.3390/rs9090929>.
- "Canopy 2014." 2016. <https://www.arcgis.com/sharing/rest/content/items/05cbf1630c2f4904a076298b888dinfo/metadata/metadata.xml?format=default&output=html>.
- City of Portland. 2020. "Carbon Emissions." <https://www.portland.gov/bps/scg/scg-dashboard/carbon-emissions>.
- Cohen, Jacob. 1960. "A Coefficient of Agreement for Nominal Scales." <https://journals.sagepub.com/doi/abs/10.1177/001316446002000104?journalCode=epma>.
- DiSalvo, Angie, Julie Fukuda, Jeff Ramsey, and Portland Parks. 2017. "Street Tree Inventory Report: City of Portland."
- Donovan, Geoffrey, and David Butry. 2009. "The Value of Shade: Estimating the Effect of Urban Trees on Summertime Electricity Use." *Energy and Buildings* 41 (June): 662–68. <https://doi.org/10.1016/j.enbuild.2009.01.002>.
- Drennen, Ari. 2020. "Climate Deniers in the 117th Congress." *Center for American Progress*. <https://www.americanprogress.org/article/climate-deniers-117th-congress/>.
- Fang, Fang, Brenden McNeil, Timothy Warner, Gregory Dahle, and Earl Eutsler. 2020. "Street tree health from space? An evaluation using WorldView-3 data and the Washington D.C. Street Tree Spatial Database." *Urban forestry & urban greening* 49: 126634–34. <https://doi.org/10.1016/j.ufug.2020.126634>.

- Flint, Harrison L. 1985. "Plants Showing Tolerance of Urban Stress." *Journal of Environmental Horticulture* 3 (2): 85–89. <https://doi.org/10.24266/0738-2898-3.2.85>.
- @GrumpyReviewer2. 2020. "The Growing Inaccessibility of Science #AcademicTwitter @AcademicChatter #Phdlife #Phdcgat #Ecrchat <Https://t.co/5JnzFBMdym>." <Https://twitter.com/GrumpyReviewer2/status/1283728846525612033>.
- Huang, Cho-ying, William R. L. Anderegg, and Gregory P. Asner. 2019. "Remote Sensing of Forest Die-Off in the Anthropocene: From Plant Ecophysiology to Canopy Structure." *Remote Sensing of Environment* 231 (September): 111233. <Https://doi.org/10.1016/j.rse.2019.111233>.
- James, Peter, Rachel F. Banay, Jaime E. Hart, and Francine Laden. 2015. "A Review of the Health Benefits of Greenness." *Current Epidemiology Reports* 2 (2): 131–42. <Https://doi.org/10.1007/s40471-015-0043-7>.
- Khorram, Siamak. 2012. *Remote Sensing*. 1st ed. 2012. SpringerBriefs in Space Development. New York, NY: Springer New York : Imprint: Springer.
- Lazarus, Michael, Chelsea Chandler, and Peter Erickson. 2013. "A Core Framework and Scenario for Deep GHG Reductions at the City Scale." *Energy Policy* 57 (June): 563–74. <Https://doi.org/10.1016/j.enpol.2013.02.031>.
- Markman, Art. 2018. "Why People Aren't Motivated to Address Climate Change." *Harvard Business Review*. <Https://hbr.org/2018/10/why-people-arent-motivated-to-address-climate-change>.
- McConville, Kelly. 2020. *pdxTrees: Data Package of Portland, Oregon Trees*. <Https://github.com/mcconvil/pdxTrees>.
- McHugh, Mary L. 2012. "Interrater Reliability: The Kappa Statistic." *Biochimia Medica* 22 (3): 276–82. <Https://www.ncbi.nlm.nih.gov/pmc/articles/PMC3900052/>.
- Moore, Gerald K. 1979. "What Is a Picture Worth? A History of Remote Sensing / Quelle Est La Valeur d'une Image? Un Tour d'horizon de Télédétection." *Hydrological Sciences Bulletin* 24 (4): 477–85. <Https://doi.org/10.1080/02626667909491887>.
- Myneni, R., F. Hall, P. Sellers, and A. Marshak. 1995. "The Interpretation of Spectral Vegetation Indexes." *IEEE Transactions on Geoscience and Remote Sensing*. <Https://doi.org/10.1109/36.377948>.
- Nowak, David J., and Daniel E. Crane. 2002. "Carbon Storage and Sequestration by Urban Trees in the USA." *Environmental Pollution* 116 (3): 381–89. [Https://doi.org/10.1016/S0269-7491\(01\)00214-7](Https://doi.org/10.1016/S0269-7491(01)00214-7).
- Nowak, David J., Daniel E. Crane, and Jack C. Stevens. 2006. "Air Pollution Removal by Urban Trees and Shrubs in the United States." *Urban Forestry & Urban Greening* 4 (3): 115–23. <Https://doi.org/10.1016/j.ufug.2006.01.007>.
- Nowak, David J., Eric J. Greenfield, Robert E. Hoehn, and Elizabeth Lapoint. 2013. "Carbon Storage and Sequestration by Trees in Urban and Community Areas of the United States." *Environmental Pollution* 178 (July): 229–36. <Https://doi.org/10.1016/j.envpol.2013.03.019>.
- Nowak, David J, Susan M Stein, Paula B Randler, Sara J Comas, Mary A Carr, and Ralph J Alig. 2010. "Sustaining America's Urban Trees and Forests."
- Planet. n.d. "Calculate an NDVI in Python: Learn to Calculate a Vegetation Index to Assess the Quality of Vegetation Within an Area of Interest." <Https://developers.planet.com/>

- planetschool/calculate-an-ndvi-in-python/.
- “Planet Imagery Product Specifications.” 2022, March. https://assets.planet.com/docs/Planet_Combined_Imagery_Product_Specs_letter_screen.pdf.
- Plowright, Andrew, and Jean-Romain Roussel. 2021. *ForestTools: Analyzing Remotely Sensed Forest Data*. <https://github.com/andrew-plowright/ForestTools>.
- Portland Urban Forestry. 2019. “Inventory Findings 2019,” October. <https://www.portland.gov/trees/get-involved/tree-summit>.
- Ripley, Brian. 2021. *MASS: Support Functions and Datasets for Venables and Ripley’s MASS*. <http://www.stats.ox.ac.uk/pub/MASS4/>.
- Robertson, Guy, and Andy Mason, eds. 2016. “Assessing the Sustainability of Agricultural and Urban Forests in the United States.” *USDA Forest Service FS-1067, 75 Pp.*, no. FS-1067. <http://www.fs.usda.gov/treesearch/pubs/52278>.
- Safford, Hannah, Elizabeth Larry, E. Gregory McPherson, David J. Nowak, and L. M. Westphal. 2013. “Urban Forests and Climate Change.” <https://www.fs.usda.gov/ccrc/topics/urban-forests>.
- Sander, Heather, Stephen Polasky, and Robert G. Haight. 2010. “The Value of Urban Tree Cover: A Hedonic Property Price Model in Ramsey and Dakota Counties, Minnesota, USA.” *Ecological Economics* 69 (8): 1646–56. <https://doi.org/10.1016/j.ecolecon.2010.03.011>.
- Schlegel, Benjamin, and Marco Steenbergen. 2020. *Brant: Test for Parallel Regression Assumption*. <https://benjaminschlegel.ch/r;brant/>.
- Schroeder, H., and W. N. Cannon. 1983. “The Esthetic Contribution of Trees to Residential Streets in Ohio Towns.” *Undefined*. <https://www.semanticscholar.org/paper/The-esthetic-contribution-of-trees-to-residential-Schroeder-Cannon/76ab66281fa734ae7106cc7794310b5463cb8f77>.
- Schroeder, Herbert W. 2011. “Does Beauty Still Matter? Experiential and Utilitarian Values of Urban Trees.” In: *Trees, People and the Built Environment. Proceedings of the Urban Trees Research Conference; 2011 April 13-14; Edgbaston, Birmingham, UK. Institute of Chartered Foresters: 159-165.*, 159–65. <http://www.fs.usda.gov/treesearch/pubs/41349>.
- Schroeder, Herbert W, and William N Cannon. 1987. “Visual Quality of Residential Streets: Both Street and Yard Trees Make a Difference,” 5.
- Selbig, William R., Steven P. Loheide, William Shuster, Bryant C. Scharenbroch, Robert C. Coville, James Kruegler, William Avery, Ralph Haefner, and David Nowak. 2021. “Quantifying the Stormwater Runoff Volume Reduction Benefits of Urban Street Tree Canopy.” *Science of The Total Environment*, October, 151296. <https://doi.org/10.1016/j.scitotenv.2021.151296>.
- Shi, Cheng Hua, Dr Youn-Jeng Choi, Qingzhou. n.d. *Companion to BER 642: Advanced Regression Methods*. https://bookdown.org/chua/ber642_advanced_regression/.
- “Smart Trees Collaboratory.” 2022. <https://www.pdx.edu/digital-city/smart-trees-collaboratory>.
- Taylor, Andrea Faber, Frances E. Kuo, and William Sullivan. 2002. “Views of Nature and Self Discipline: Evidence from Inner City Children.” *Journal of Environmental Psychology* 22 (1): 49–63. <https://doi.org/10.1006/jevp.2001.0241>.
- Taylor, Andrea Faber, Frances E. Kuo, and William C. Sullivan. 2001. “Coping with ADD: The Surprising Connection to Green Play Settings.” *Environment and Behavior* 33 (1): 54–77.

- <https://doi.org/10.1177/00139160121972864>.
- Trope, Yaacov, and Nira Liberman. 2010. "Construal-Level Theory of Psychological Distance." *Psychological Review* 117 (2): 440–63. <https://doi.org/10.1037/a0018963>.
- Tsoka, Stella, Thomas Leduc, and Auline Rodler. 2021. "Assessing the Effects of Urban Street Trees on Building Cooling Energy Needs: The Role of Foliage Density and Planting Pattern." *Sustainable Cities and Society* 65 (February): 102633. <https://doi.org/10.1016/j.scs.2020.102633>.
- Tucker, Compton J. 1979. "Red and Photographic Infrared Linear Combinations for Monitoring Vegetation." *Remote Sensing of Environment* 8 (2): 127–50. [https://doi.org/10.1016/0034-4257\(79\)90013-0](https://doi.org/10.1016/0034-4257(79)90013-0).
- United Nations, Department of Economics, and Social Affairs. 2018. "68." <https://www.un.org/development/desa/en/news/population/2018-revision-of-world-urbanization-prospects.html>.
- US EPA. 2020. "Urbanization and Storm Water Runoff." <https://www.epa.gov/sourcewaterprotection/urbanization-and-storm-water-runoff>.
- USDA Forest Service, Northern Research Station. 2011. "Urban Tree Canopy Analysis Helps Urban Planners With Tree Planting Campaigns." *NRS Research Review* 13: 6.
- Venables, W. N., and B. D. Ripley. 2002. *Modern Applied Statistics with s*. Fourth. New York: Springer. <https://www.stats.ox.ac.uk/pub/MASS4/>.
- Ward, Kathleen T., and Gary R. Johnson. 2007. "Geospatial Methods Provide Timely and Comprehensive Urban Forest Information." *Urban Forestry & Urban Greening* 6 (1): 15–22. <https://doi.org/10.1016/j.ufug.2006.11.002>.
- Xiao, Qingfu, and E. Gregory McPherson. 2005. "Tree Health Mapping with Multispectral Remote Sensing Data at UC Davis, California." *Urban Ecosystems* 8 (3-4): 349–61. <https://doi.org/10.1007/s11252-005-4867-7>.